Chapter 5: Mechanistic DFT investigation of catalytic oxidation of NO to NO_2 on pristine and doped $[Au_nPd_{3-n}]^-$ (n=0-3) clusters.

Abstract

In our previous chapter, it was found that $[Au\text{-}Pd]^-$ acts as an efficient catalyst towards the catalytic conversion of NO into NO_2. Hence, in Chapter 5, pristine and doped anionic $[Au_nPd_{3-n}]^-$ (n=0-3) trimer clusters were chosen to comprehend the oxidation mechanism of NO into NO_2 at the molecular level. Our aim is to find the effect of addition of one atom on the catalytic efficiency of the clusters. Again, combination of M06L/def2TZVP method is applied in order to compare the results with the previous chapters. Pristine and doped anionic $[Au_nPd_{3-n}]^-$ (n=0-3) clusters were chosen as gas-phase Au clusters are ideal model systems for imitating gold catalysts as they have electronic structure similar to active supported gold catalysts. Based on the co-adsorption energies, the detailed reaction routes under the Langmuir Hinshelwood (LH), termolecular Eley-Rideal (TER), and termolecular Langmuir Hinshelwood (TLH) mechanisms were explored, in which two NO molecules are converted to two NO_2 molecules using molecular O_2. Results show that on doping Pd on anionic $[Au_3]^-$clusters, adsorption of both NO and O_2 increases. Our calculations show that Pd site on bimetallic clusters is more preferable for adsorption than that of Au site. Moreover, energetic span model reveals $[Au_2Pd]^-$cluster to be the most efficient cluster towards conversion of NO to NO_2 via L-H mechanism. Hence, the addition of one atom decreases the activation barrier and increases the catalytic efficiency.

Graphical Abstract

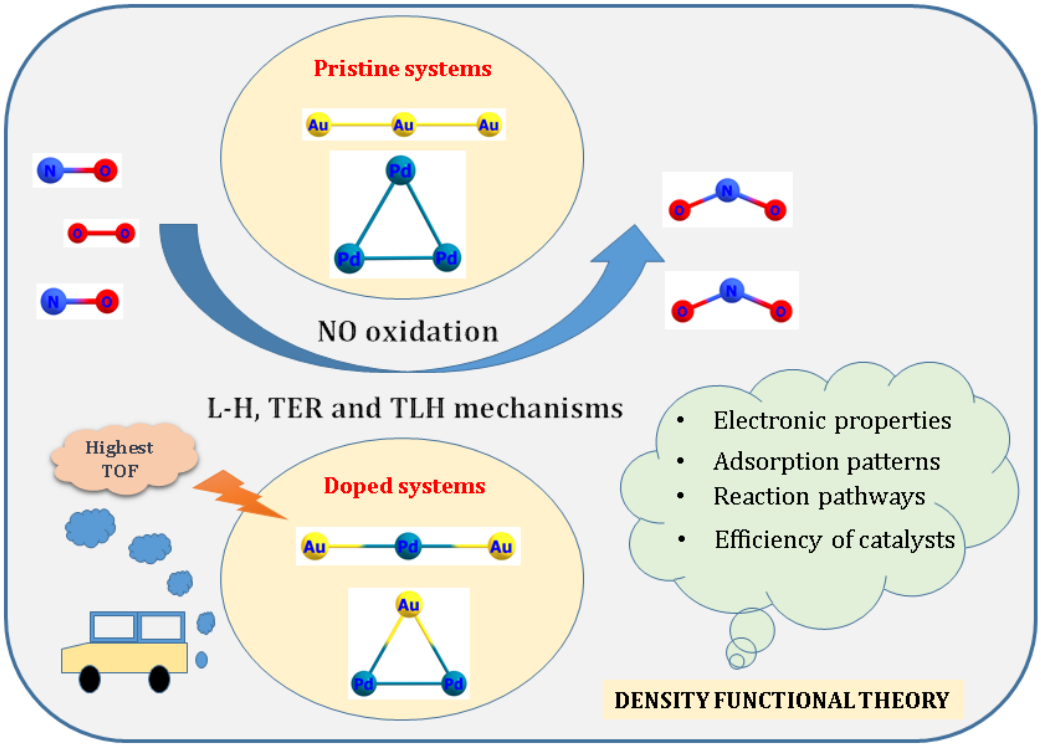

5.1 Introduction

Nitrogen Oxides (NO_x), which mostly consist of nitric oxide (NO) and nitrogen dioxide (NO_2), are one of the primary air pollutants in the world, causing acid rain, ozone depletion, and photochemical smog [1, 2]. Nitric oxide accounts for more than 90 percent of NO_x and is the cause of serious respiratory ailments [3]. As a result, chemically converting NO to N_2 is critical for preventing air pollution. NO oxidation to NO_2 is a key process in NO_x abatement technologies such as selective catalytic reduction (SCR), continuously regenerating trap (CRT) and NO_x storage and reduction (NSR). Among all the techniques available, NH_3-SCR is widely regarded as the most effective technology for lowering NO_x emissions in the presence of excess oxygen [4, 5]. The rate of the NH_3-SCR reaction can be considerably boosted if a fraction of the NO is transformed into NO_2. At low temperatures (200-300 °C), the "fast" SCR reaction ($4NH_3 + 2NO + 2NO_2 \rightarrow 4N_2 + 6H_2O$) is approximately 10 times faster than the normal NO and NH_3 reaction ($4NH_3 + 4NO + O_2 \rightarrow 4N_2 + 6H_2O$) [6, 7]. Hence, it has been established that the oxidation of NO to NO_2 ($2NO + O_2 \rightarrow 2NO_2$) is a critical step in NH_3- SCR. Compared to other oxidants used for oxidation of NO such as O_3 [8, 9], H_2O_2 [10, 11], $KMnO_4$ [12] etc., molecular oxygen acts as a green, non-toxic and inexpensive oxidant. Under usual circumstances, the oxidation of NO is somewhat slow due to the complicated chemical composition of the fuel gas and the varied particle size distributions [13]. Therefore, a lot of effort has been put into designing catalysts that are suitable for NO oxidation.

Although platinum, palladium, and rhodium are the most commonly used catalysts for the aforementioned processes, substantial study has revealed that gold also has potential applications in this field. Gold-based catalysts have the potential to solve “cold-start” problem in the automobile as they perform better than those of platinum group metals at low temperatures [14, 15]. Furthermore, lean burn engines are becoming increasingly popular since they provide the most cost-effective and practical solution to reduce NO_x emissions. Various materials such as zeolites, metal oxides etc. have been investigated to operate the catalytic processes, however, dispersed Au catalysts are considered one of the promising catalysts for practical emission reduction on lean burn engines [16, 17]. Au/Al_2O_3, Au/TiO_2, and Au/CeO_2 are examples of gold catalysts that exhibit remarkable low-

temperature performance and great selectivity in reducing nitrogen oxides to N_2 [18, 19]. Some believe that in the future, gold catalysts could probably take the place of platinum group ones [17, 20]. In addition, Au catalysts have become one of the most promising catalysts for a number of other significant chemical processes such as CO oxidation [21, 22] propylene epoxidation [23], water-gas shift reaction [24, 25] etc.

Recently, an alternative approach has been adopted for designing specific catalysts for selective oxidation processes, which is to use small metal clusters made up of only a few atoms and having catalytic characteristics unique from those of isolated metal cations and bulk metals [26-28]. Metal atoms and clusters exhibit high reactivity in a variety of chemical processes [29, 30] and also serves as perfect podiums for studying the mechanisms of complex reactions. Unsupported nanosized Au particles have been demonstrated to be active catalysts [31, 32], implying that the catalytic activity may be inherent in nano- or sub-nanogold particles. Due to charge transfer from supports to deposited gold clusters, the electronic structure of free anionic gold clusters are expected to be similar to that of the active supported gold catalysts [33]. Hence, Au_n^- clusters perfectly mimic the environment of supported Au catalysts [34].

The interactions between gold clusters and the reactants (O_2 and NO) are important to investigate, as activation of both reactants is a key step in the oxidation of NO. Several investigations have been done to study the chemical reactivity between Au clusters and O_2 [35-39]. Cox *et al*. [35] reported the first experimental study on the chemical interactions of neutral, cationic, and anionic gas-phase Au_n clusters with O_2. They found out that anionic clusters with even n are more reactive towards O_2 compared to cationic and neutral clusters. Huang *et al*. [36] did organized analysis of the interactions between O_2 and Au_n^- (n = 1−7) using photoelectron spectroscopy and found out that molecular chemisorption of O_2 occurs on Au_n^- for n = 2, 4, 6 and physisorption of O_2 takes place for odd sized Au_n^- (n = 3, 5, 7) clusters. Fielicke and co-workers [37] investigated geometrical structures using infrared multiphoton desorption spectroscopy and observed the vibrational spectra of $Au_nO_2^-$ (n = 4, 6, 8, 10, 12, 14, 18, and 20). The adsorption and activation of NO on Au clusters of different sizes has also been the subject of

numerous investigations [40-44]. Citra *et al.* [40] reported experimental as well as theoretical study of NO adsorption on single Au atom in which they found that gold reacts strongly with nitric oxide to form AuNO and $Au(NO)_2$ products. A systematic DFT analysis of NO interaction with Au clusters up to n = 6 was carried out by Ding *et al.* [41].They observed that all Au clusters, with the exception of Au_3^-, adsorb NO, regardless of their charge state. Multiple NO adsorption study on $Au_{1-12}^-$was conducted, and it was discovered that disproportionate reaction products $Au_nNO_2^-$ were formed for the sizes with n = 4, 6, and 8 [43]. The same group extended their studies [44] on the adsorption and reaction of NO on the anionic Au clusters with sizes upto 1 nm and concluded that NO adsorption was dominated by the clusters' spins, and most even sizes with open electron shells were reactive.

One way to enhance the catalytic activity of gold clusters is to alloy with a metal that is miscible and has a synergistic influence on the nature of Au. Pd–Au bimetallic alloy catalysts has drawn a lot of interest lately due to its superior activity in a wide range of reactions such as low temperature CO oxidation [45, 46], direct H_2O_2 synthesis from H_2 and O_2 [47, 48], hydrogenation of hydrocarbons [49] etc. Particularly, for CO oxidation, studies have shown that when Pd is mixed with Au, they show better catalytic activity corresponding to their monometallic counterparts [50-51]. Peng *et al.* [50] studied CO adsorption and oxidation on Au_mPd_n (m + n = 2–6) bimetallic clusters and found that the calculated reaction barrier of CO oxidation was lower for Au_2Pd than those of Au_3 and Pd_3. Wu and coworkers [51] found that the reaction barrier for CO oxidation is relatively lower for AuPd (111) than that of pure Pd (111) surface slab and the addition of Au significantly improves the activity of a Pd–Au bimetallic slab for CO oxidation. However, very limited research is available when it comes to NO oxidation on AuPd bimetallic system [52, 53]. Our previous study [53] have demonstrated that AuPd anionic dimer is capable of oxidizing two NO molecules to two NO_2 molecules using molecular O_2 via L-H mechanism. For this reason, we are interested to know if AuPd anionic trimer may accomplish the same objective at a lower reaction barrier.

In this work, we put forward for the first time NO oxidation employing gas phase $[Au_nPd_{3-n}]^-$(n=0-3) mono and bimetallic trimers via LH, TER and TLH mechanisms. Previous studies [35, 36, 41] have indicated $[Au_3]^-$ trimer to be less

reactive towards O_2 and NO. However, it is expected that chemical bonding of $[Au_3]^-$ cluster towards the same molecules may increase on alloying it with Pd atoms. Hence, a detailed theoretical study has been carried out for the titled reaction to

(1) finding the adsorption and co-adsorption pattern of NO and O_2 molecules

(2) providing deep insights into the oxidation mechanism of nitric oxide on pure and doped anionic gold dimers and

(3) finding the effect of alloying a pure Au_3 cluster with Pd atoms and how it modifies its electronic environment and its catalytic activity towards NO oxidation.

The findings from our study will aid in understanding the oxidation process at the molecular level, providing new perspectives for the development of a class of catalysts with high catalytic activity and maximum atom utilization.

5.2 Computational Details

DFT calculations are carried out using the Gaussian 09 software package [54] to produce optimized structures, ground state energies, and frequencies for every species. For the entire calculation, a combination of density fitting triple zeta valence with single-polarization (def2TZVP) [55-56] basis set and a more widely used M06L [57] local density functional are selected. The M06L functional has been shown to be reliable on predicting and exploring the properties of precious metals accurately, particularly Au [53, 58-60]. According to vibrational frequency calculations, stable intermediate species have all positive frequencies while TSs have a single imaginary frequency. A transition state structure's (TSs) geometry is optimized using either the synchronous transit-guided quasi-Newton (STQN) method [61] or the Berny algorithm [62].The reliability of the reaction path that links the transition state with its two nearby intermediates has been verified through IRC calculations [63]. Effect of mixing in binary alloys are determined by calculating the excess energy Δ given by-

$$\Delta = NE_{Au_m Pd_n} - mE_{Au_N} - nE_{Pd_N} \quad (1)$$

Where $E_{Au_m Pd_n}$ is the total zero-point corrected energy of the binary alloy and E_{Au_N} and E_{Pd_N} are the total zero-point corrected energies of the pure Au_N and Pd_N

(M=Pd, Pt), respectively. Here N is equal to 3. The negative value of excess energy suggests beneficial mixing, whereas the positive value shows a demixing tendency.

The adsorption energy (E_{ads}) of NO and O_2 on $[Au_nPd_{3-n}]^-$(n=0-3) has been calculated using the equation-

$$E_{ads} = E_{trimers/NO/O_2} - (E_{trimers} + E_{NO/O_2}) \quad (2)$$

where $E_{trimers}$ represents the total zero-point corrected energy of the $[Au_nPd_{3-n}]^-$(n=0-3) trimers, E_{NO/O_2} is the total zero-point corrected energy of the NO/O_2 molecule and $E_{trimers/NO/O_2}$ is the total zero-point corrected energy of the NO/O_2 adsorbed on trimers. Natural Bond Orbital (NBO) [64] calculations have been carried out at the same theoretical level to investigate the chemical behavior of the reactants and pure catalysts. Moreover, Multiwfn program [65] is used to analyze the orbital composition of the HOMO-LUMO isosurfaces of the clusters.

The energetic span model (ESM), originally derived from the Arrhenius Eyring transition state theory, and is used to evaluate the efficiency of different clusters. The model is developed and put into practical use by Kozuch and Shaik [66-68].This model expresses turnover frequency (TOF) as a function of catalytic energy span (δE). The model suggests that instead of a rate-determining step, the catalytic cycle uses rate-determining states to determine the cycle's apparent activation energy. The transition state and intermediate responsible for the apparent activation energy are referred to as turnover frequency-determining transition state (TDTS) and turnover frequency-determining intermediate (TDI).

$$TOF = \frac{K_B T}{h} e^{-\frac{\delta E}{RT}} \quad (3)$$

Eq. (2) describes the link between TOF and energy span (δE). K_B is Boltzmann's constant, T is the room temperature, h is Planck's constant, and R is the gas constant.

$$\delta E = \begin{pmatrix} T_{TDTS} - I_{TDI}, \text{ if TDTS appears after TDI} \\ T_{TDTS} - I_{TDI} + \Delta G_r, \text{ if TDTS appears before TDI} \end{pmatrix} \quad (4)$$

Eq. (3) illustrates the connection between energy span (δE), TOF determining transition state (TDTS), and TOF determining intermediate.

5.3 Results and Discussion

5.3.1 Electronic structures and energies of the $[Au_nPd_{3-n}]^-$(n=0-3) clusters

Figure 5.1 shows ground state electronic structures of $[Au_3]^-$, $[Au_2Pd]^-$, $[AuPd_2]^-$, $[Pd_3]^-$, NO and O_2 obtained at the M06L/def2TZVP level of theory along with their natural charges (shown in parentheses) and bond lengths (in Å).

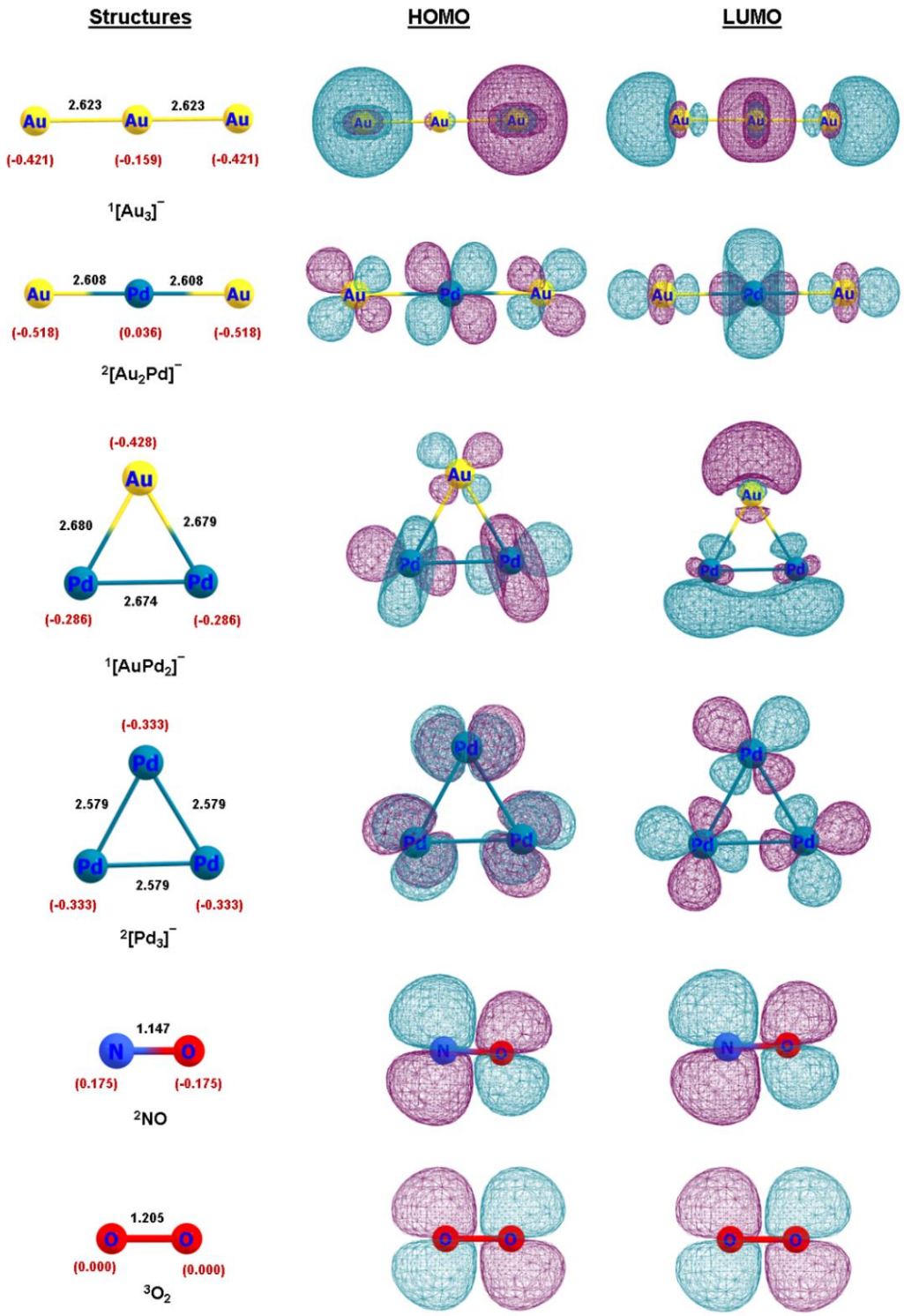

Figure 5.1: Ground state electronic structures of $[Au_3]^-$, $[Au_2Pd]^-$, $[AuPd_2]^-$, $[Pd_3]^-$, NO and O_2 obtained at the M06L/def2TZVP level of theory along with their natural charges (shown in parentheses) and bond lengths (in Å).

$[Au_3]^-$ have two configurations, linear and triangular, in which linear configuration(SM=1) is found to be the most stable structure. Further, the

difference in energy between the linear and the triangular structure of $[Au_3]^-$is 28.61 kcal/mol. The equilibrium bond-length (2.623 Å) and bond-angle (180°) of the $[Au_3]^-$cluster are consistent with previously reported results [69, 70]. The ground state structure of $[Au_2Pd]^-$cluster is linear (Figure 5.1) with $D_{\infty h}$ symmetry, having two Au-Pd bond lengths of 2.608 Å which is in good agreement as reported by Ai-Jie *et al.*[71]. On increasing the spin state from ground doublet state to quartet spin state, the structure remains the same; however energy increases up to 58.42 kcal/mol. Moreover, the energy difference between the linear and triangular structure of $[Au_2Pd]^-$cluster is only 1.85 kcal/mol. The optimized structure of $[AuPd_2]^-$ is found to be triangular (Figure 5.1) having C_{2v} symmetry with singlet spin as a ground state structure. A linear structure is also obtained for $[AuPd_2]^-$ cluster in the form Pd-Au-Pd which is 20.56 kcal/mol more in energy than the triangular ground state structure. Finally, the ground state structure obtained for pure $[Pd_3]^-$ trimer is an equilateral triangle (D_{3h} symmetry) with angles of 60^0 and sides with equal bond lengths of 2.578 Å [72, 73]. The quartet spin state structure is also a triangular structure which is 26.34 kcal/mol more energy than the doublet ground state structure. A linear structure is also obtained which is 28.54 kcal/mol higher in energy. The bond lengths of NO, O_2, and NO_2 are found to be 1.147 Å, 1.205 Å, and 1.191 Å, respectively. These values are similar to those given in the CRC Handbook of Chemistry and Physics [74]. For bimetallic trimers ($[Au_2Pd]^-$ and $[AuPd_2]^-$), the excess energy is found to be positive, thus, indicating demixing tendency for Au and Pd.

5.3.2 Molecular orbital analysis and electronic properties of the $[Au_nPd_{3-n}]^-$ (n=0-3) clusters

Figure 5.1 includes the orientation of HOMO and LUMO of the $[Au_nPd_{3-n}]^-$ (n=0-3) clusters and the reactants along with their optimized geometries. For ground spin multiplicity other than singlet, there is a possibility for HOMO and LUMO to have same or different spin channels. $[Au_3]^-$ and $[AuPd_2]^-$ have singlet multiplicity. For $[Au_2Pd]^-$ as well as $[Pd_3]^-$ clusters, both HOMO-LUMO belongs to β spin channel {HOMO(β), LUMO(β)}. The cluster's HOMO and LUMO should be discussed since they provide insight into how the cluster bonds to the reactants. In $[Au_3]^-$, 6s orbitals of the terminal Au atoms are the major contributors in both HOMO as well as LUMO.

For HOMO, the middle Au atom contributed very little via $6p_z$ and $5d_z^2$orbitals. Natural charge indicates that the terminal atoms are more negative compared to the middle Au atom. Both molecular orbital analysis and natural charge analysis indicates bonding of $[Au_3]^-$ cluster with reactants via terminal Au atoms. In $[Au_2Pd]^-$ cluster, the HOMO is largely concentrated on the $4d_{yz}$ orbital of the Pd atom (67.88%) while two terminal Au contributed roughly around 32% via $5d_{yz}$ orbital. The LUMO is largely distributed among the $5d_z^2$and 5sorbitals of Pd atoms where $5d_z^2$ is the major contributor. Au being more electronegative, the electronic charge resides on the two Au atoms. However, orbital analysis indicates that the frontier orbitals resides on the Pd atom present in the $[Au_2Pd]^-$cluster. Hence, it can be said that the bonding of the reactants may occur on the Pd site of the $[Au_2Pd]^-$cluster. $[AuPd_2]^-$trimer consists of HOMO fully spread out in the two Pd atoms present in the cluster with the major contributions from the $[AuPd_2]^-$ trimer consists of HOMO entirely distributed out in the two Pd atoms in the cluster, with the main contributions from $4d_{x2-y2}$ and$4d_z^2$ orbitals. For LUMO, Au contributes roughly around 33% via 6s and $6p_y$ orbitals and the remaining part is distributed among the two Pd atoms where 5s is the main contributor orbital. The HOMO of $[Pd_3]^-$cluster is well distributed among each Pd atoms with contributions from $4d_{xz}$ and $4d_{yz}$ orbitals. Even distribution can also be seen for LUMO with contributions from $4d_{xy}$ and $4d_{x2-y2}$ orbitals. Table 5.1 provides orbital's contribution to the HOMO and LUMO of each cluster.

Table 5.1: Contribution of each orbital to the HOMO and LUMO of $[Au_nPd_{3-n}]^-$ (n=0-3) clusters.

	Center	**Label**	**Type**	**Composition**
$[Au_3]^-$**_HOMO**	1(Au)	s	Val(6s)	44.636 %
	3(Au)	s	Val(6s)	44.636 %
$[Au_3]^-$**_LUMO**	1(Au)	s	Val(6s)	21.261 %
	2(Au)	s	Val(6s)	37.088 %
	3(Au)	s	Val(6s)	21.261 %
$[Au_2Pd]^-$**_HOMO**	1(Au)	d_{yz}	Val(5d)	15.761 %

	2(Pd)	d_{yz}	Val(4d)	67.881 %
	3(Au)	d_{yz}	Val(5d)	15.769 %
$[Au_2Pd]^-$**_LUMO**	1(Au)	d_{z2}	Val(5d)	7.801 %
	2(Pd)	s	Val(5s)	12.131 %
	2(Pd)	d_{z2}	Val(4d)	66.569 %
	3(Au)	d_{z2}	Val(5d)	7.806 %
$[AuPd_2]^-$**_HOMO**	1(Pd)	d_{xy}	Val(4d)	9.351 %
	1(Pd)	d_{x2-y2}	Val(4d)	22.553 %
	1(Pd)	d_{z2}	Val(4d)	13.550 %
	2(Pd)	d_{xy}	Val(4d)	9.351 %
	2(Pd)	d_{x2-y2}	Val(4d)	22.544 %
	2(Pd)	d_{z2}	Val(4d)	13.550 %
$[AuPd_2]^-$**_LUMO**	1(Pd)	s	Val(5s)	25.837 %
	2(Pd)	s	Val(5s)	25.837 %
	3(Au)	s	Val(6s)	26.843 %
$[Pd_3]^-$**_HOMO**	1(Pd)	d_{xz}	Val(4d)	33.328 %
	2(Pd)	d_{xz}	Val(4d)	8.335 %
	2(Pd)	d_{yz}	Val(4d)	25.000 %
	3(Pd)	d_{xz}	Val(4d)	8.335 %
	3(Pd)	d_{yz}	Val(4d)	25.000 %
$[Pd_3]^-$**_LUMO**	1(Pd)	d_{xy}	Val(4d)	33.074 %
	2(Pd)	d_{xy}	Val(4d)	8.266 %
	2(Pd)	d_{x2-y2}	Val(4d)	24.800 %
	3(Pd)	d_{xy}	Val(4d)	8.266 %
	3(Pd)	d_{x2-y2}	Val(4d)	24.800 %

Another crucial factor to consider is the cluster's electronic properties, which provide useful information about their chemical reactivity. Table 5.2 includes electronic properties of the $[Au_nPd_{3-n}]^-$ (n=0-3) clusters(HOMO-LUMO gap=HLG), Ionization potential =IP and Electron Affinity= EA). HLG follows the order: $[Au_3]^-$>$[AuPd_2]^-$>$[Au_2Pd]^-$>$[Pd_3]^-$. Table 5.2 shows that doping Pd to $[Au_3]^-$ cluster results in a considerable decrease in HLG values. Since HLG value is associated with stability, the most stable and least reactive cluster is anticipated to be $[Au_3]^-$. Conversely, the most reactive species is anticipated to be the $[Pd_3]^-$cluster. The similar pattern is also shown by the values of softness and hardness. However, other electronic properties such as electronegativity and chemical potential indicating $[Au_2Pd]^-$ cluster to be the most reactive one. However, these are preliminary observations and investigating the full reaction pathways is necessary to determine the reactivity of these clusters.

Table 5.2: Electronic properties of $[Au_nPd_{3-n}]^-$ (n=0-3) clusters at the M06L/def2TZVP level of theory.(HOMO-LUMO gap (HLG), Ionization potential (IP) and Electron Affinity (EA)).

Catalyst	Properties (in eV)						
	HLG	IP	EA	Hardness	Softness	Electro-negativity	Chemical Potential
$[Au_3]^-$	2.385	1.137	-1.248	1.192	0.419	0.055	-0.055
$[Au_2Pd]^-$	0.542	0.856	0.313	0.271	1.842	-0.584	0.584
$[AuPd_2]^-$	0.560	-1.169	-1.730	0.280	1.783	1.449	-1.449
$[Pd_3]^-$	0.404	-1.100	-1.504	0.202	2.474	1.302	-1.302

5.3.3 NO/O_2 adsorption properties on $[Au_nPd_{3-n}]^-$ (n=0-3) clusters

Adsorption analysis is an important tool as it provides information about the catalyst's reactivity sites and how reactants interact with them. The reactants and catalysts must interact in an optimum nature, that is, neither too strong nor too weak, for the reaction to proceed. Optimized geometries of single NO and O_2 adsorbed on mono as well as bimetallic clusters are shown in Figure 5.2 along with

the bond parameters (in Å). Table 5.3 includes single adsorption energies of NO/O_2 adsorbed on the pure and doped Au_3 clusters.

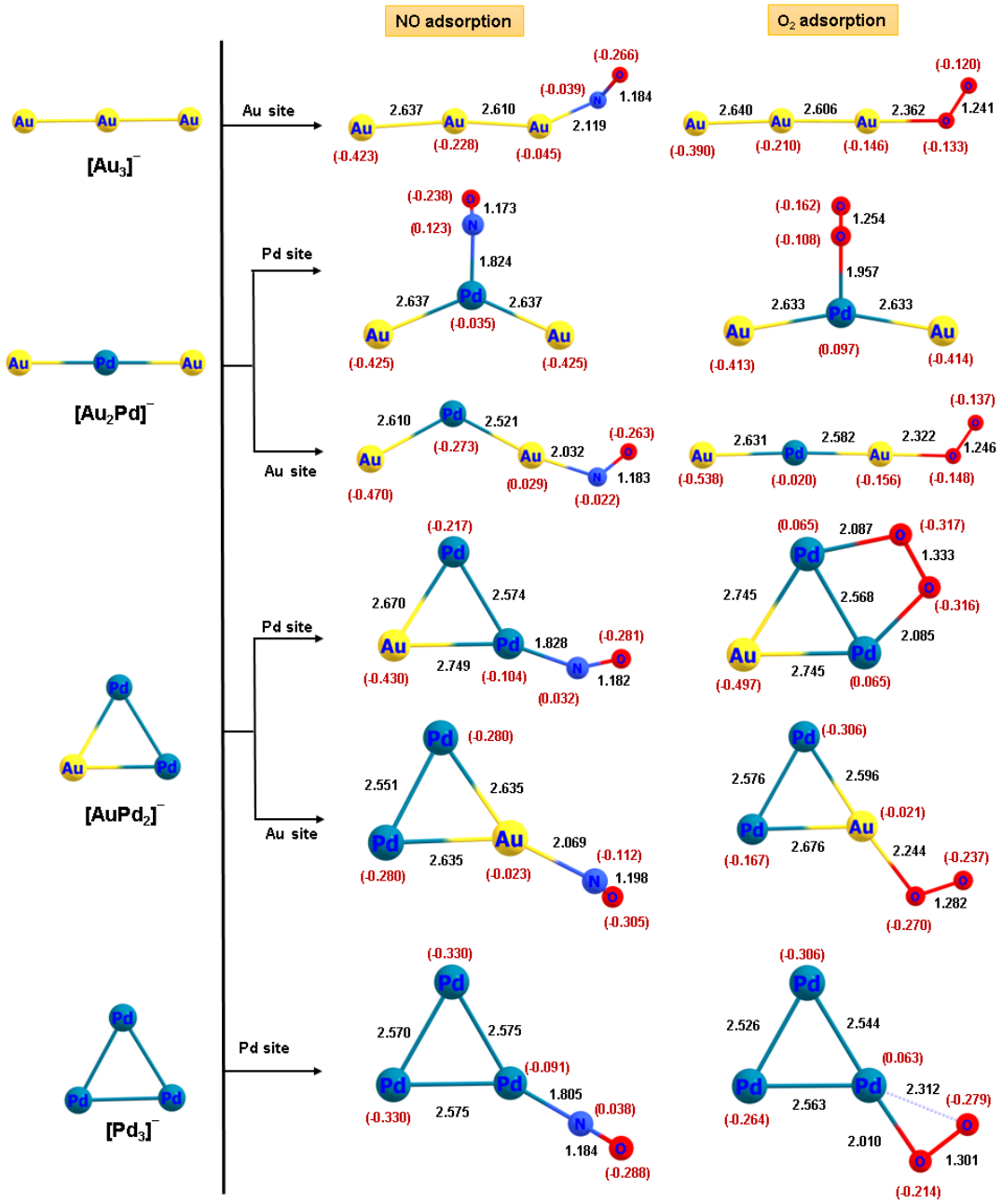

Figure 5.2: Optimized geometries of NO/O_2 adsorbed on $[Au_nPd_{3-n}]^-$ (n=0-3) clusters along with the bond parameters (in Å) at M06L/def2TZVP level.

From the natural (or NBO) charge (given in Figure 5.1), it can be perceived that the electronic charge resides on the terminal Au atoms of $[Au_3]^-$cluster. The prediction is supported by the fact that both NO and O_2 tends to bond on the terminal Au atoms of anionic Au_3 cluster. NO is bonded to one of the terminal Au

atom in an end-on position with an adsorption energy (E_{ads}) of about -14.54 kcal/mol (Table 5.3). The structure and E_{ads} of NO adsorbed on $[Au_3]^-$cluster is consistent with the previously reported result [41]. In a similar fashion, O_2 is bonded in an end-on position to one of the terminal Au atom with adsorption energy of -5.87 kcal/mol [36, 69]. It is seen that the adsorption energies of NO and O_2 adsorbed on $[Au_3]^-$cluster is very small. It is due to the odd-even effect observed for the anionic clusters. Odd sized anionic clusters are found to be inert towards reactants such as O_2 due to their closed shell electronic structure [36, 69]. $[Au_2Pd]^-$and $[AuPd_2]^-$clusters have two possible active sites, Au site and Pd site. In case of $[Au_2Pd]^-$, due to more electronegativity of Au, electronic charges are residing in the terminal Au atoms rather than that of middle Pd atom. However, HOMO-LUMO analysis indicates that both HOMO and LUMO are mostly located on Pd site. The value of adsorption energies of NO and O_2 on the Pd site are significantly negative than that of the Au site (Table 5.3). Hence, adsorption of both NO and O_2 are preferable on Pd site for $[Au_2Pd]^-$ cluster. It is seen that after adsorbing NO on Pd site, structure of $[Au_2Pd]^-$ cluster changes from linear (180^0) to bent (130^0). When NO adsorbs on Au site, ∠Au-Pd-Au decreases from 180^0 to 123^0. In $[AuPd_2]^-$cluster, it is expected that the reactants will bond via one of the Pd atoms as most of the HOMO-LUMO contributions are from two Pd atoms. The conclusion is supported by the adsorption energies of the reactants on $[AuPd_2]^-$cluster. Both NO and O_2 binds strongly on the Pd site rather than that of Au site. NO binds to both the Pd and Au site of $[AuPd_2]^-$cluster in an end-on position with E_{ads} of about -54.53 kcal/mol and -27.53 kcal/mol, respectively. O_2 binds to Au in an end-on position (E_{ads}=-18.48 kcal/mol) whereas it binds to two Pd atoms in a bridging manner (E_{ads}=-44.95 kcal/mol). Further, both NO and O_2 adsorbs on $[Pd_3]^-$ using end-on configuration. The adsorption energies of NO and O_2 are -56.12 kcal/mol and -32.69 kcal/mol, respectively.

Table 5.3: Calculated single adsorption energy (E_{ads}) (in kcal/mol) of NO/O_2 adsorbed on the pure and doped $[Au_nPd_{3-n}]^-$ (n=0-3) clusters.

Catalyst	Adsorption sites	Spin	E_{ads}(NO)	Spin	E_{ads} (O_2)
$[Au_3]^-$	Au	2	**-14.54**	3	**-5.87**
$[Au_2Pd]^-$	Au	1	-13.34	2	0.73

	Pd	1	**-43.48**	2	**-9.14**
$[AuPd_2]^-$	Au	2	-27.53	3	-18.48
	Pd	2	**-54.53**	3	**-44.95**
$[Pd_3]^-$	Pd	1	**-56.12**	2	**-32.69**

From NBO analysis, Wiberg bond index (WBI) [75] analysis is carried out to obtain the comparative scale for the bond strength (Table 5.4). When NO adsorbs on the Pd site of the $[Au_2Pd]^-$ cluster, the WBI value for the Pd-N bond is 0.824, more than the WBI value (0.746) for the Au-N bond when NO is adsorbed on Au site. WBI is suggesting stronger Pd-N interaction in comparison to Au-N interaction. For O_2 adsorption on both the active site of $[Au_2Pd]^-$ catalyst, Pd-O bond has a WBI value of 0.369, while Au-O bond has a WBI value of 0.230. This indicates strong interaction of Pd with O atom of O_2 as compared to Au. This scenario is similar for $[AuPd_2]^-$ catalyst where WBI values of Pd-N bond and Pd-O bond are greater than that of Au-N and Au-O bond, suggesting stronger bonding of NO and O_2 with Pd site rather than Au site (Table 5.4). This results are in correlation with the adsorption energies found on $[Au_2Pd]^-$and $[AuPd_2]^-$ catalyst.

NO prefers to bind with the catalysts using its nitrogen atom in order to avoid large formal negative large on a more electronegative oxygen atom. We have also observed that the NO adsorption energies on the clusters are more negative than that of O_2 adsorption energies as NO is a good π acceptor which can accept electronic charge from metal filled d orbitals to its antibonding π* orbitals, thus strengthening the metal-nitrogen bond.

Table 5.4: Wiberg bond index (WBI) for newly formed bonds after adsorption of NO and O_2on $[Au_nPd_{3-n}]^-$ (n=0-3) clusters at M06L/def2TZVP level.

Adsorbed Species	**Wiberg bond index**					
	$[Au_3]^-$	**$[Au_2Pd]^-$**		**$[AuPd_2]^-$**		**$[Pd_3]^-$**
	Au-N	Au-N	Pd-N	Au-N	Pd-N	Pd-N
NO adsorbed	0.437	0.746	0.824	0.473	0.791	0.900
	Au-O	Au-O	Pd-O	Au-O	Pd-O	Pd-O

O_2 adsorbed	0.276	0.230	0.369	0.189	0.453;0.365	0.494

Flue gas contains both NO and O_2, so it's important to examine the various combinations of the co-adsorption of O_2 and NO molecules, as well as two NO and two O_2 molecules. The co-adsorption could occur at the same site or at the adjacent sites. Single adsorption energies of NO/O_2on $[Au_2Pd]^-$ and $[AuPd_2]^-$ clusters have shown us that the co-adsorption of both the reactants will prominently take place on Pd sites of these clusters. Since, there is only one Pd site on $[Au_2Pd]^-$cluster, there is only one configuration possible for the co-adsorption. For $[AuPd_2]^-$cluster, there are two active Pd sites; hence, the reactants may co-adsorb either on same Pd atom or on two Pd sites adjacently. In $[Au_3]^-$ cluster, terminal Au atoms are more active which means the two reactants may occupy either one or two terminal atoms, thus, leading to two different configurations. For $[Pd_3]^-$, two configurations are possible based on the adsorption location of the reactants. Table 5.5 includes co-adsorption energies (Co-E_{ads}) (in kcal/mol) of various combinations of NO and O_2 on $[Au_nPd_{3-n}]^-$ (n=0-3) clusters at M06L/def2TZVP level. From Table 5.5, it can be concluded that co-adsorption of the reactants at different sites is more favorable compared to co-adsorption at the same site (or atom). Moreover, the co-adsorption of two NO molecules are highly probable since its co-adsorption energies (Co-E_{ads}) in each cluster are very high. Our calculated adsorption as well as co-adsorption energies is in consistent with the previously reported results [76-79]. The co-adsorption modes of NO/O_2 and 2NO adsorbed on $[Au_nPd_{3-n}]^-$ (n=0-3) clusters are shown in Figure 5.3 and Figure 5.4, respectively.

Table 5.5: Calculated Co-adsorption energies (Co-E_{ads}) (in kcal/mol) of NO and O_2, two NO and two O_2 molecules co-adsorbed on different sites of $[Au_nPd_{3-n}]^-$ (n=0-3) clusters.

Catalyst	**$[Au_3]^-$**		**$[Au_2Pd]^-$**		**$[AuPd_2]^-$**		**$[Pd_3]^-$**	
	Spin	**Co-E_{ads}**	**Spin**	**Co-E_{ads}**	**Spin**	**Co-E_{ads}**	**Spin**	**Co-E_{ads}**
NO & O_2 (same_site)	2	-20.54	3	-38.25	2	-69.77	3	-59.62
NO & O_2	2	-22.85	---	---	1	-90.26	3	-82.46

(diff_site)								
2 NO (same_site)	3	-25.23	4	-41.35	3	-95.44	2	-91.90
2 NO (diff_site)	3	-30.91	---	---	1	-103.44	2	-102.95
2 O_2 (same_site)	3	1.25	2	-41.20	1	-54.93	2	-52.65
2 O_2 (diff_site)	3	-12.03	---	---	3	-69.11	4	-58.26

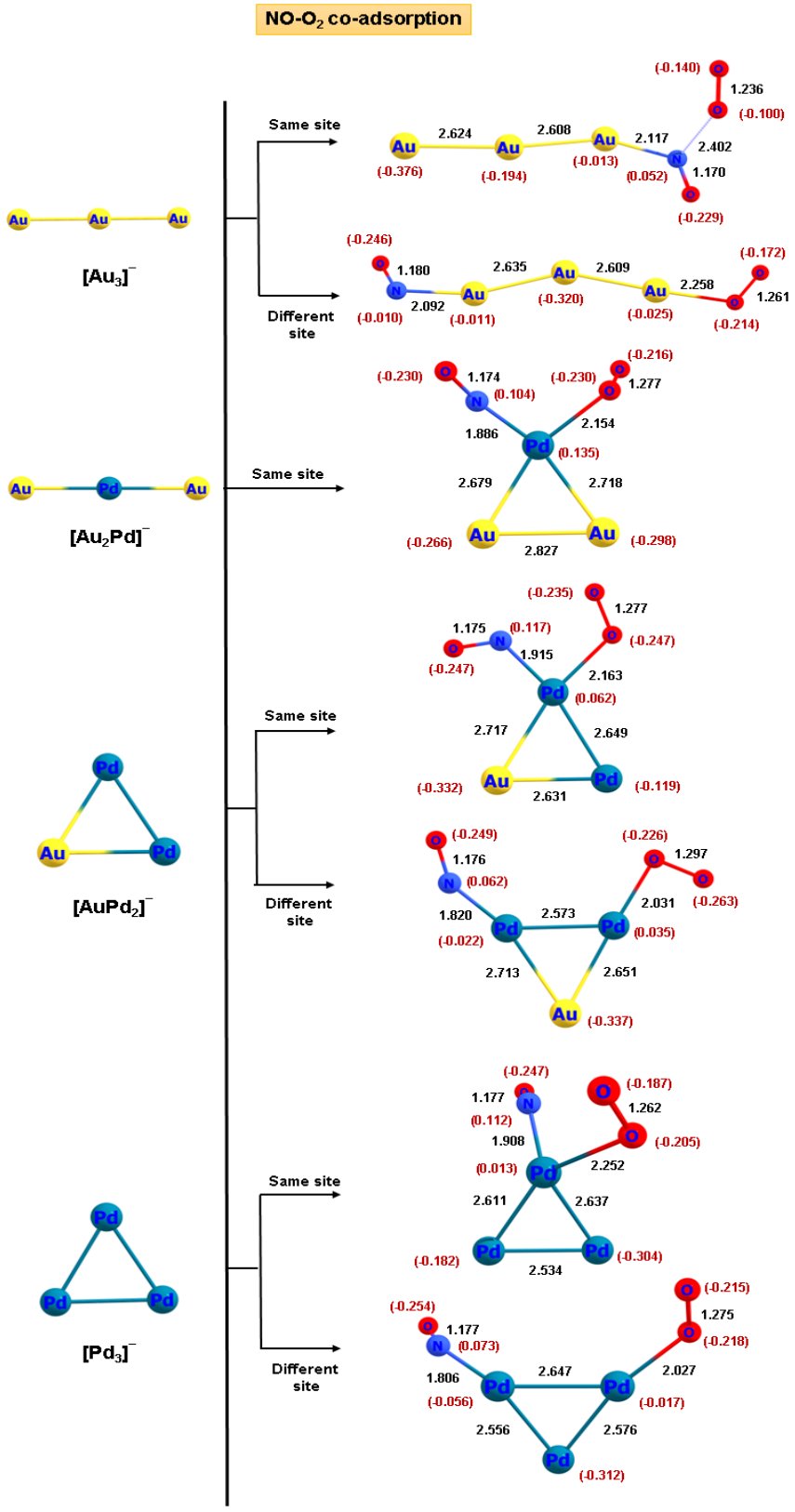

Figure 5.3: Optimized geometries of NO and O_2 co-adsorbed on $[Au_nPd_{3-n}]^-$ (n=0-3) clusters at M06L/def2TZVP level along with the bond parameters (in Å) and NBO charges (given in parentheses).

For $[Au_3]^-$ cluster, the difference between Co-E_{ads} of NO and O_2 at the same site and different site is very less (2.31 kcal/mol). For same site adsorption, it is seen that O_2 is not directly linked to the catalyst; rather it is weakly bonded to NO. The bond length (d_{O-O}) and vibrational frequency (ν_{O-O}) of O_2 in this configuration are 1.236 Å and 1424.66 cm^{-1}, respectively. In case of different site adsorption, both NO and O_2 are adsorbed to different terminal Au atoms. The d_{O-O} and $\nu_{O-O}$for different site adsorption are 1.261 Å and 1304.27 cm^{-1}, respectively. Hence, it becomes evident that O_2 gets activated more in case of different site adsorption. Similar scenario is obtained for NO where it is activated more in case of different site adsorption (d_{N-O}=1.180 Å and ν_{N-O}=1674.23cm^{-1}). Table 5.6 contains values of vibrational frequencies and WBI. $[Au_2Pd]^-$ have only one active site, so there is only one configuration (same site configuration). It is interesting to note that on doping Pd atom on $[Au_3]^-$ cluster, the Co-E_{ads} of NO and O_2 increases. Moreover, the $[Au_2Pd]^-$ cluster structure changes from linear to triangle upon co-adsorption. The Co-E_{ads} of NO and O_2, 2NO and $2O_2$ are nearly the same for $[Au_2Pd]^-$ cluster which means that competition may occur between all the various configurations to occur. In case of same site adsorption of NO and O_2 on $[Au_2Pd]^-$, the values of ν_{N-O} and ν_{O-O} are 1708.49 cm^{-1} and 1243.95 cm^{-1}, respectively, which indicates redshift in frequency. For $[AuPd_2]^-$ cluster, the Co-E_{ads} values of NO and O_2 at the same site and different site are -69.77 kcal/mol and -90.26 kcal/mol, respectively. These values suggests that the probability of NO and O_2 co-adsorbing on different site is more. Table 5 suggests higher activation of O_2 (d_{O-O} =1.297 Å and ν_{O-O} =1203.61cm^{-1}) on different site configuration. Similar is the case for $[Pd_3]^-$ cluster where the Co-E_{ads} of NO and O_2 is higher in case of different site adsorption. The ν_{O-O} for same site configuration is 1298.93 cm^{-1} whereas for different site adsorption, the value of $\nu_{O-O}$is 1260.52 cm^{-1}. This indicates more activation and more redshift in frequency for O_2 in case of different site adsorption. For NO, the redshift in frequency is occurring more in case of same site adsorption (1679.88 cm^{-1}).

Table 5.6: Vibrational frequencies (in cm^{-1}) and Wiberg bond indexes (WBI) for co-adsorption of NO and O_2 on $[Au_nPd_{3-n}]^-$ (n=0-3) clusters.

Catalyst	Same site co-adsorption		Different site co-adsorption	
$[Au_3]^-$	ν_{N-O}	WBI_{N-O}	ν_{N-O}	WBI_{N-O}
	1715.12	1.832	1674.23	1.827
	ν_{O-O}	WBI_{O-O}	ν_{O-O}	WBI_{O-O}
	1424.66	1.402	1304.27	1.334
$[Au_2Pd]^-$	ν_{N-O}	WBI_{N-O}	ν_{N-O}	WBI_{N-O}
	1708.49	1.828	---	---
	ν_{O-O}	WBI_{O-O}	ν_{O-O}	WBI_{O-O}
	1243.95	1.305	---	---
$[AuPd_2]^-$	ν_{N-O}	WBI_{N-O}	ν_{N-O}	WBI_{N-O}
	1696.00	1.833	1750.87	1.805
	ν_{O-O}	WBI_{O-O}	ν_{O-O}	WBI_{O-O}
	1272.67	1.298	1203.61	1.262
$[Pd_3]^-$	ν_{N-O}	WBI_{N-O}	ν_{N-O}	WBI_{N-O}
	1679.88	1.827	1731.34	1.771
	ν_{O-O}	WBI_{O-O}	ν_{O-O}	WBI_{O-O}
	1298.93	1.335	1260.52	1.229

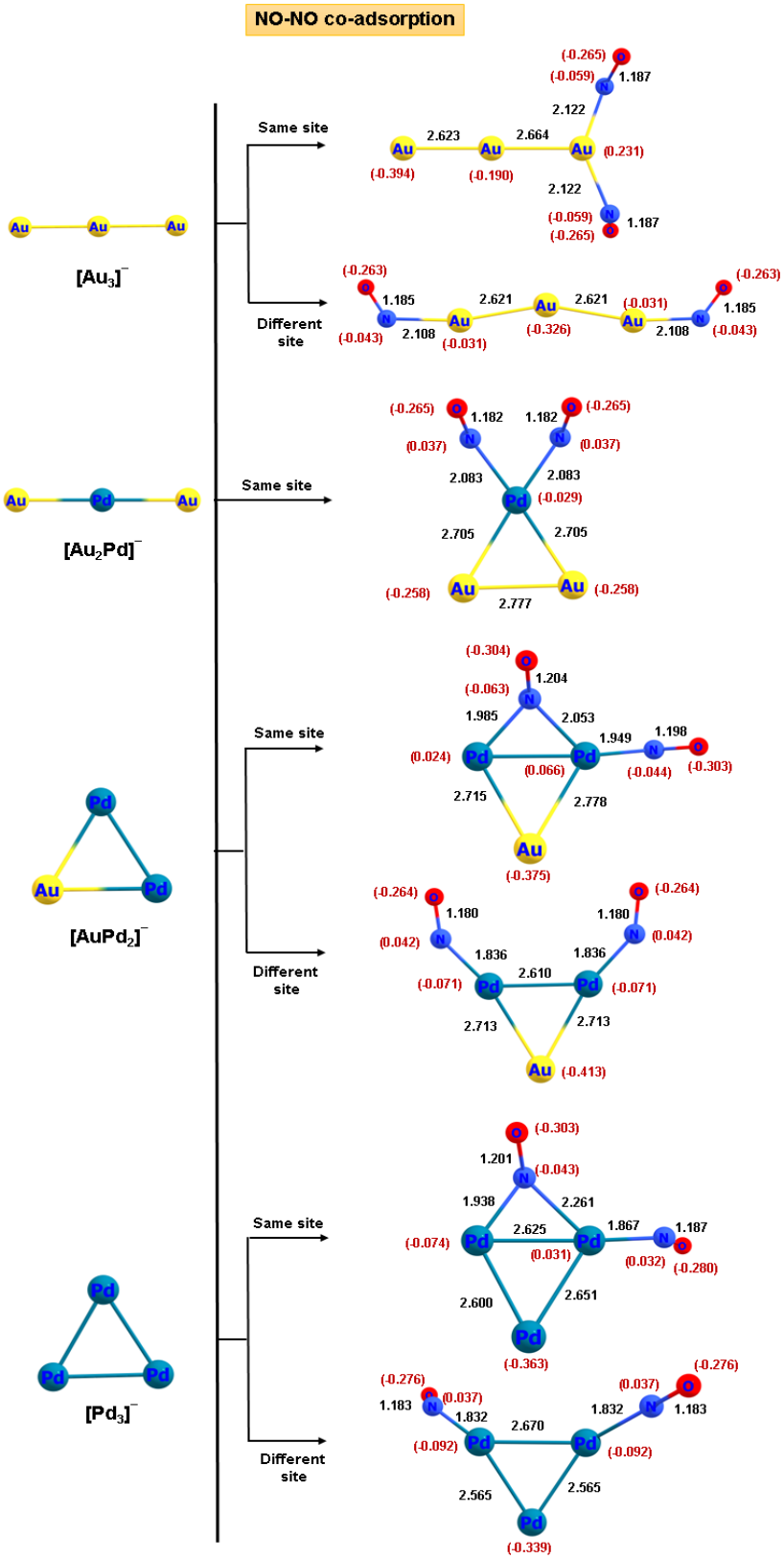
NO-NO co-adsorption
[Au3]−
Same site
Different site
[Au2Pd]−
Same site
[AuPd2]−
Same site
Different site
[Pd3]−
Same site
Different site

Figure 5.4: Optimized geometries of two NO co-adsorbed on $[Au_nPd_{3-n}]^-$ (n=0-3) clusters at M06L/def2TZVP level along with the bond parameters (in Å) and NBO charges (given in parentheses).

When it comes to $[Au_3]^-$cluster, the energy difference between two NO molecules co-adsorbed on different terminal Au atoms and the same terminal Au atom is 5.68 kcal/mol. For adsorption on same site, looking at the natural charge of terminal Au (0.231e), it is evident that electron transfer has occurred from Au orbitals to π* orbital of NO. Consequently, NO experiences elongation, as indicated by its bond lengths (1.187 Å) and ν_{N-O} (1658.54 cm^{-1}). Table 5.7 contains values of vibrational frequencies and WBI. Similar is the case for co-adsorption at different terminal Au sites where NO bond lengths (1.185 Å) and vibrational frequencies (1682.57 cm^{-1}) also suggesting activation of NO. When two NO molecules co-adsorb on the $[Au_2Pd]^-$ cluster, the cluster's structure changes from linear to triangular. Co-adsorption of two NO molecules on Pd site of the cluster leads to its activation which is evident from redshift in frequencies (1719.20 cm^{-1}). The configuration for the same site adsorption on $[AuPd_2]^-$ cluster and $[Pd_3]^-$ cluster is similar where one NO molecule is in bridged configuration and another NO is in linear position. Looking at Table 6, it is confirmed that the bridged NO is more activated in comparison to the linear NO for both the clusters. For $[AuPd_2]^-$ cluster, the Co-E_{ads} of two NO molecules co-adsorbed on different site is more (-103.44 kcal/mol) than that of co-adsorption on the same site (-95.44 kcal/mol) which signifies that two NO molecules prefer to co-adsorb adjacently. However, the difference in energy between two configurations is less which means that presence of both the configurations is possible. Similar is the case for $[Pd_3]^-$ cluster where Co-E_{ads} of two NO molecules co-adsorbed on different site is more (Table 5.5) and the difference in energy between the two configurations is less (11.05 kcal/mol). However, Table 5.7 shows that same site co-adsorption is activating NO molecules much more than the different site co-adsorptions.

Table 5.7: Vibrational frequencies (in cm^{-1}) and Wiberg bond indexes (WBI) for co-adsorption of two NO molecules on $[Au_nPd_{3-n}]^-$ (n=0-3) clusters.

Catalyst	Same site co-adsorption	Different site co-adsorption

$[Au_3]^-$	ν_{N-O}	WBI_{N-O}	ν_{N-O}	WBI_{N-O}
	1658.54	1.807	1682.57	1.761
$[Au_2Pd]^-$	ν_{N-O}	WBI_{N-O}	ν_{N-O}	WBI_{N-O}
	1719.20	1.157	---	---
$[AuPd_2]^-$	ν_{N-O}	WBI_{N-O}	ν_{N-O}	WBI_{N-O}
	1541.03;1631.81	1.659;1.702	1740.62	1.920
$[Pd_3]^-$	ν_{N-O}	WBI_{N-O}	ν_{N-O}	WBI_{N-O}
	1535.83;1665.83	1.621;1.878	1718.23	1.749

It is to note that NO and O_2 adsorbed at the same site and different sites give rise to conventional Langmuir-Hinshelwood mechanism, L-H_{ss} (ss=same site) and L-H_{ds} (ds=different sites) respectively. Whereas co-adsorption of two NO molecules can give rise to Termolecular Eley Rideal (TER) and Termolecular Langmuir Hinshelwood mechanism (TLH). Co-adsorption of two O_2 molecules doesn't lead to any type of mechanism and thus, not discussed in details. Based on the adsorption sites of the reactants, these mechanisms can be categorized into TER_{ss}, TER_{ds}, TLH_{ss} and TLH_{ds}. In our study, L-H, TER and TLH mechanisms have been taken into consideration for catalytic oxidation of NO on $[Au_nPd_{3-n}]^-$ (n=0-3) clusters owing to their single as well as co-adsorption energies of the reactants**.** Eley-Rideal (E-R) mechanism is not taken into consideration as for E-R mechanism to occur, the adsorption of O_2becomes very important. Since, adsorption energies of O_2 adsorbed on the trimers is much lower as compared to that of NO, the probability of E-R mechanism occurring is very low.

5.3.4 Catalytic oxidation pathway of NO on $[Au_nPd_{3-n}]^-$ (n=0-3) clusters

5.3.4.1 Langmuir Hinshelwood (L-H) mechanism

Langmuir Hinshelwood (L-H) is a conventional bimolecular mechanism where co-adsorption of both the reactants are important. In case of NO oxidation,

activation of both the reactants, that is, NO and O_2 is required to facilitate the formation of NO_2. For reaction to proceed smoothly, optimum adsorption energy of the reactant onto the catalyst is of utmost importance as low adsorption energy will not make the reaction go forward and higher adsorption energy will poison the catalyst. Previous studies have shown L-H mechanism to be an efficient mechanism for NO oxidation [53, 79-81]. The co-adsorption of NO and O_2 on the same site (or atom) results in L-H_{ss} (ss=same site) whereas co-adsorption of NO and O_2 on different sites (or atoms) results in L-H_{ds} (ds=different sites). L-H_{ss} mechanism undergoes via three steps: (i) Interaction of NO and O_2on the same site and formation of O-N-O-O bond (TS1):(ii) Breaking of the newly formed O-N-O-O bond to form first NO_2 (TS2) and (iii) Incoming of second NO and formation of the second NO_2 (TS3). Figure 5.5 (a), (b), (c) and (d) represents the optimized geometries of intermediates and transition states involved in the NO oxidation pathway via LH_{ss} on $[Au_nPd_{3-n}]^-$ (n=0-3) clusters, respectively. Figure 5.6 demonstrates the potential energy surface (PES) profile for the LH_{ss} mechanism. The relative Gibbs' free energies of all the intermediates and transition states have been calculated with respect to $[Au_nPd_{3-n}]^-$ (n=0-3) + 2NO (gas) + O_2 (gas) at 298.15K and 1 atm.

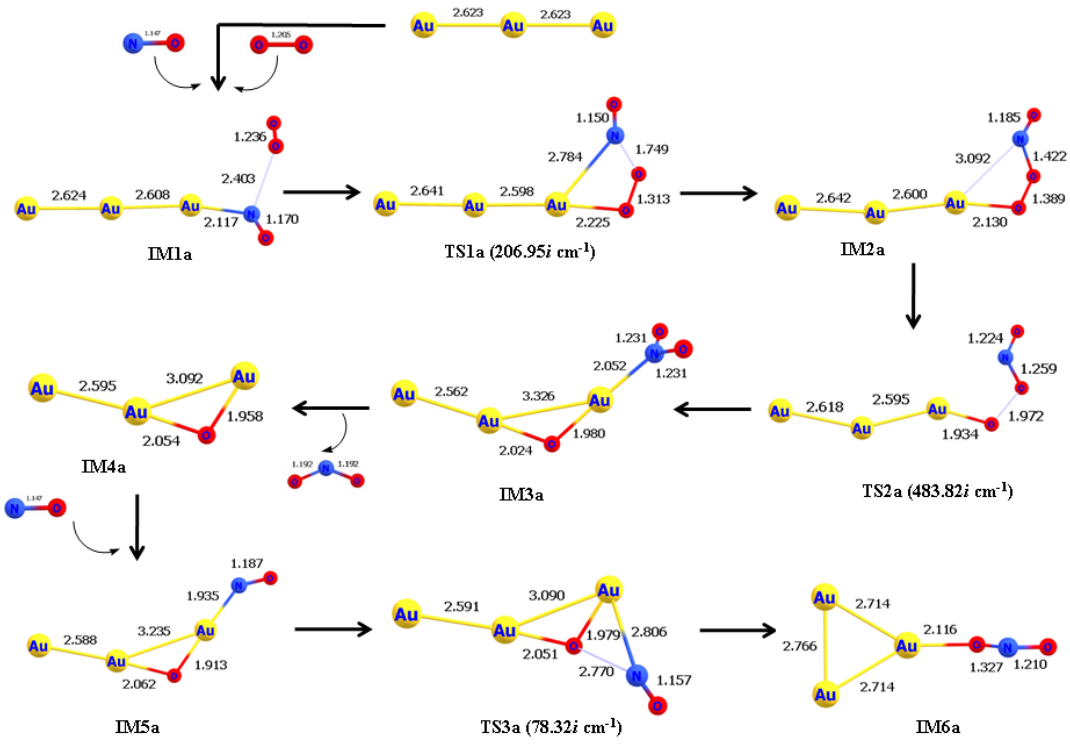

(a)

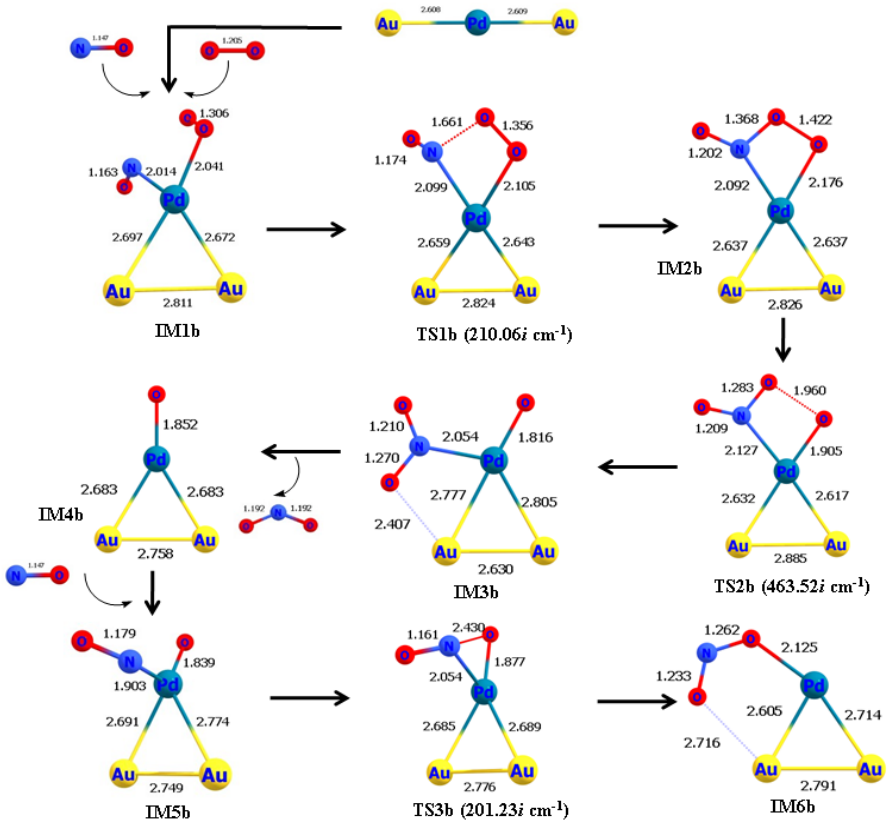
IM1b
TS1b (210.06*i* cm^{-1})
IM2b
TS2b (463.52*i* cm^{-1})
IM3b
IM4b
IM5b
TS3b (201.23*i* cm^{-1})
IM6b

(b)

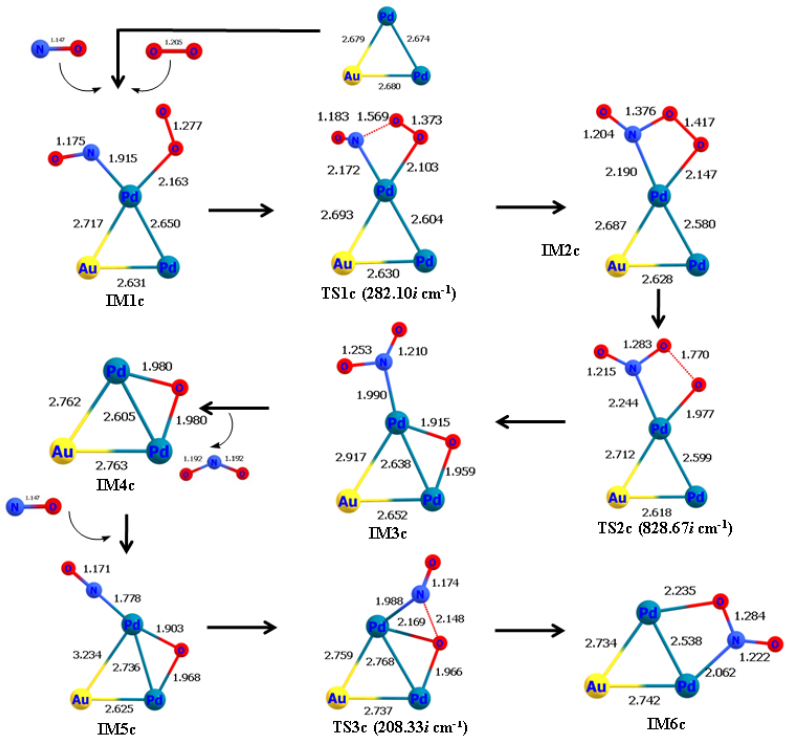
IM1c
TS1c (282.10*i* cm^{-1})
IM2c
TS2c (828.67*i* cm^{-1})
IM3c
IM4c
IM5c
TS3c (208.33*i* cm^{-1})
IM6c

(c)

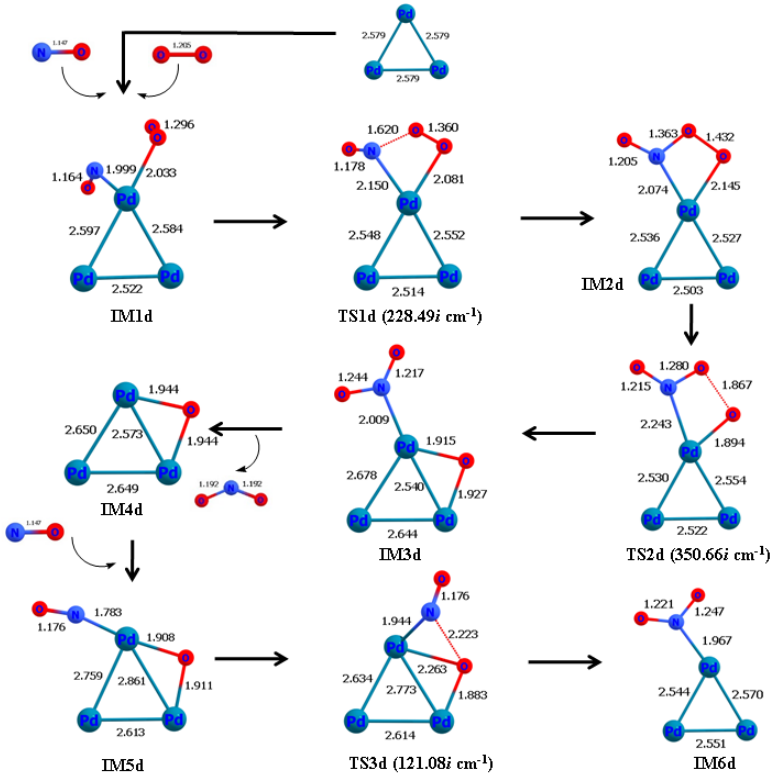

(d)

Figure 5.5: Intermediates and transition states involved in catalytic oxidation pathway of NO via LH_{ss} mechanism on (a) $[Au_3]^-$ (b) $[Au_2Pd]^-$ (c) $[AuPd_2]^-$ and (d) $[Pd_3]^-$along with their bond lengths (in Å). Imaginary frequency of each TS is given in parentheses.

The reaction starts with the co-adsorption of NO and O_2 on one of the terminal Au atoms of $[Au_3]^-$ forming IM1a. It is to be noted that O_2 is not directly linked to the cluster, rather it is weakly attached to NO. However, as the reaction proceed forward, O_2 along with NO, gets adsorbed to the catalyst and shows characteristics of an L-H mechanism. Co-adsorption of NO and O_2 on same site of $[Au_2Pd]^-$, $[AuPd_2]^-$ and $[Pd_3]^-$ give rise to IM1b, IM1c and IM1d, respectively.IM1a, IM1b, IM1c and IM1d are -5.71 kcal/mol, -29.40 kcal/mol, -51.84 kcal/mol and -31.55 kcal/mol, respectively, lower in energy than the starting point (Catalyst + Reactants). The first transition state of LH_{ss} occurs where NO and O_2 interacts with each other and form an O-N-O-O type bond structure. Looking at the bond parameters in TS1a, it becomes evident that O_2 bond is elongated (1.236 Å in IM1a to 1.313 Å in TS1a) and

a new N-O bond is to be formed. Similar scenario is occurring in TS1 (b, c and d) where elongation of O_2 molecule is taking place. Barrier height of TS1a, TS1b, TS1c and TS1d are 12.26, 2.43, 17.43 and 4.43 kcal/mol, respectively. The barrier height of TS1b for $[Au_2Pd]^-$ cluster is very low (2.43 kcal/mol). It could be explained by the fact that, during co-adsorption, O_2 in IM1b was activated most significantly (1.306 Å) among all the clusters. This step is endothermic for all the clusters, except $[Au_2Pd]^-$. Hence, first step is kinetically as well as thermodynamically favorable in $[Au_2Pd]^-$ cluster. Reaction proceed forward where O-N-O-O bond breaks to form first NO_2 molecule and a lone 'O' atom. The barrier height for TS2a, TS2b, TS2c and TS2d are 15.98, 15.58, 9.76 and 9.90 kcal/mol, respectively. This step is highly exothermic for all the clusters as shown in Figure 5.6. From Potential Energy Surface, it is clear that IM3c and IM3d are much more stable intermediate than IM3a and IM3b. The desorption of NO_2 from the system gives rise to IM4. The desorption energy E_{des} of first NO_2 is lowest for $[Au_2Pd]^-$ cluster (11.85 kcal/mol) while E_{des} of first NO_2 is 40.02 kcal/mol for $[Au_3]^-$, 42.80 kcal/mol for $[AuPd_2]^-$and 43.82 kcal/mol for $[Pd_3]^-$ cluster. After NO_2 is removed from the system, one NO enters the system, interacts with IM4 to form IM5. From PES, it is obvious that IM5c and IM5d are much more stable intermediate than IM5a and IM5b in PES which signifies that NO is strongly bonded to IM5c and IM5d. The last transition state (TS3) involves interaction of second NO with lone 'O' atom and formation of the second NO_2. The activation barrier for the formation of second NO_2 in $[Au_3]^-$ is 33.73 kcal/mol while it is 13.13 kcal/mol in $[Au_2Pd]^-$, 37.95 kcal/mol in $[AuPd_2]^-$ and 39.09 kcal/mol in $[Pd_3]^-$ cluster. Hence, kinetically, this step is feasible only on$[Au_2Pd]^-$ cluster. In $[Au_2Pd]^-$ cluster, the third step is exothermic by 25.74 kcal/mol. Therefore, $[Au_2Pd]^-$ cluster is found to be efficient in catalyzing two NO molecules to two NO_2 molecules via LH_{ss} mechanism.

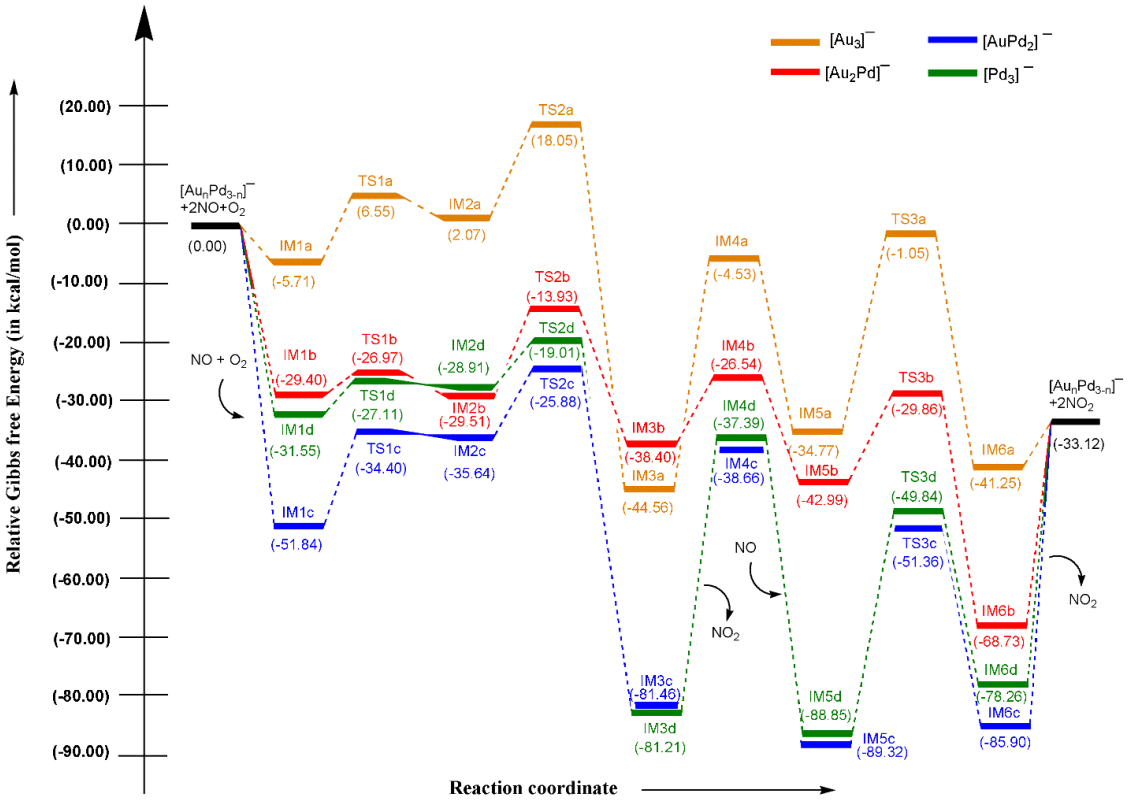

Figure 5.6: Energy profile diagram for LH_{ss} mechanism on $[Au_nPd_{3-n}]^-$ (n=0-3) clusters at M06L/def2TZVP level.

LH_{ds} mechanism undergoes via two steps: (i) Interaction of NO and O_2 adsorbed on different sites and formation of NO_2 via breaking of O-N-O-O bond (TS1/) and (ii) Incoming of second NO and formation of the second NO_2 (TS2/). Figure 5.7 (a) and (b)represents the optimized geometries of intermediates and transition states involved in the NO oxidation pathway via LH_{ss} on $[Au_nPd_{3-n}]^-$ (n=0-3) clusters, respectively. Figure 5.8 reveals the PES profile for the LH_{ds} mechanism.

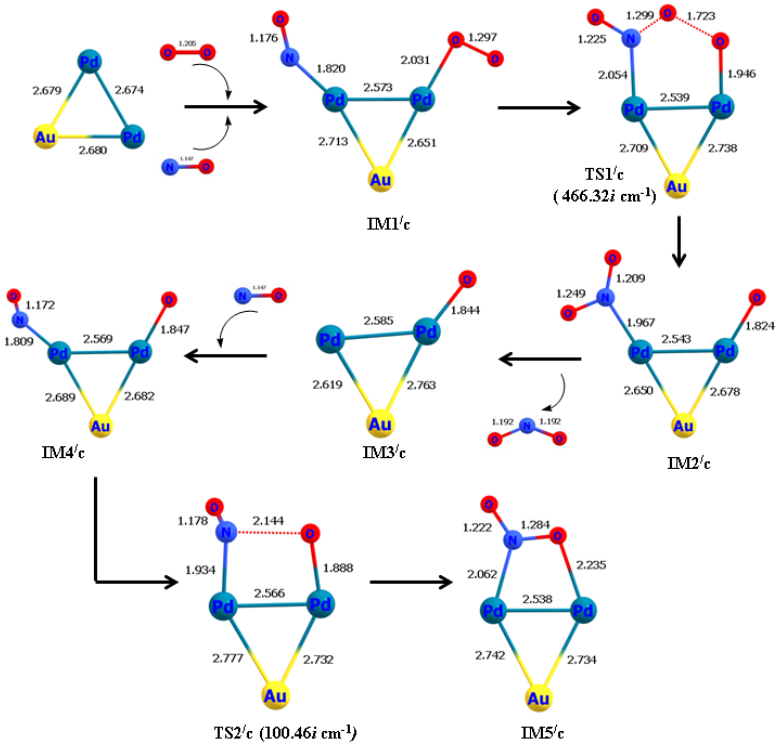

(a)

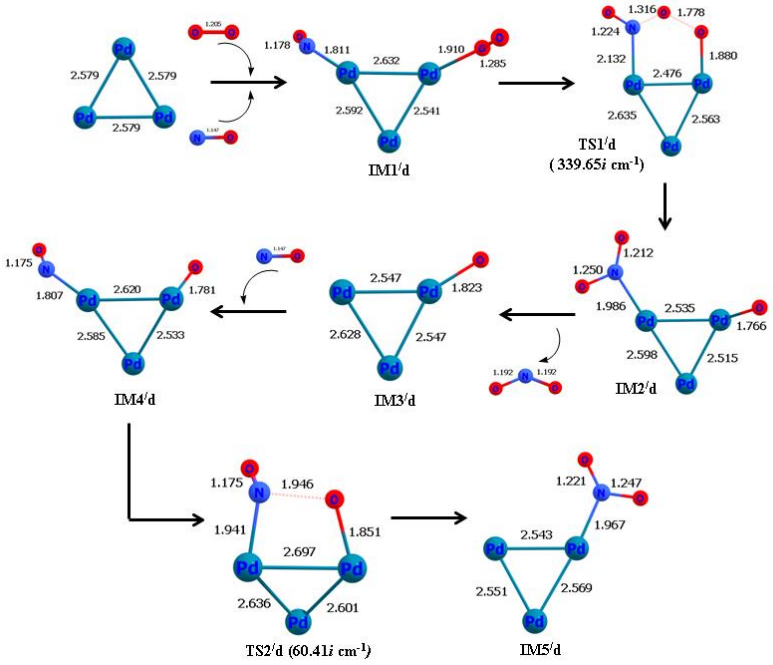

(b)

Figure 5.7: Intermediates and transition states involved in catalytic oxidation pathway of NO via LH_{ds} mechanism on (a) $[AuPd_2]^-$and (b) $[Pd_3]^-$along with their bond lengths (in Å). Imaginary frequency of each TS is given in parentheses.

LH_{ds} cannot occur in $[Au_3]^-$ system as NO and O_2 are not adjacently adsorbed in the $[Au_3]^-$ which makes the distance between NO and O_2 quite high. Hence, it becomes difficult for both the reactants to interact with each other. In case of $[Au_2Pd]^-$, since it has only one active site (Pd site), so reactants adsorbing adjacently is not favored in this trimer system, hence, LH_{ds} is not followed. LH_{ds} is followed in case of $[AuPd_2]^-$and $[Pd_3]^-$ clusters as there is a possibility of NO and O_2 adsorbing adjacently to each other in these two clusters. Reaction starts when NO and O_2 are adsorbed adjacently in the Pd atoms of $[AuPd_2]^-$ clusters, forming IM1/c. IM1/c is -72.16 kcal/mol lower in energy than the starting point. Looking at the structure of IM1/c (Figure 5.7), it is clear that upon co-adsorption, NO (1.147 Å to 1.176 Å) and O_2 (1.205 Å to 1.297 Å) are activated simultaneously. In a similar manner, side by side co-adsorption of NO and O_2 on $[Pd_3]^-$ cluster gives rise to IM1d which is -52.20 kcal/mol lower in energy in PES. Comparing the energies of IM1c and IM1d, it is obvious that co-adsorption of NO and O_2 is stronger in IM1c. Both NO (1.178 Å) and O_2 (1.285 Å) are activated in IM1d to some extent. Reaction proceeds via TS1c where one O atom of O_2 interacts with N atom of NO. O-O bond is cleaved in TS1c which is evident from its bond length (1.723 Å). The barrier height of TS1/c is 34.66 kcal/mol. Similar scenario occurs in TS1/d where O-O bond is cleaved (1.778 Å) and a new N-O bond is formed (1.316 Å). The activation barrier for TS1/d is 31.11 kcal/mol. The step is exothermic for both the clusters. IM2/c and IM2/d is formed where both NO_2 and 'O' atom are attached adjacently. After that, NO_2 leaves the $[AuPd_2]^-$cluster with desorption energy of 39.76 kcal/mol, forming IM3/c. IM3/d is formed when NO_2 leaves the $[Pd_3]^-$ cluster with desorption energy of 38.93 kcal/mol. NO enters the system and gets adsorbed adjacently to site where 'O' atom is already present, forming IM4/c and IM4/d in$[AuPd_2]^-$and $[Pd_3]^-$, respectively. Second transition state arises when NO interacts with its nearby 'O' atom, forming another NO_2. The barrier height for this step is 14.99 kcal/mol and 15.46 kcal/mol in $[AuPd_2]^-$and $[Pd_3]^-$, respectively. IM5/c and IM5/d are formed in $[AuPd_2]^-$and $[Pd_3]^-$, respectively in which NO_2 is fully formed. It is to be noted that these two intermediates are most stable species in their respective PES. Hence, desorption energies of NO_2 leaving IM5/c and IM5/d is 52.78 kcal/mol and 45.04 kcal/mol, respectively.

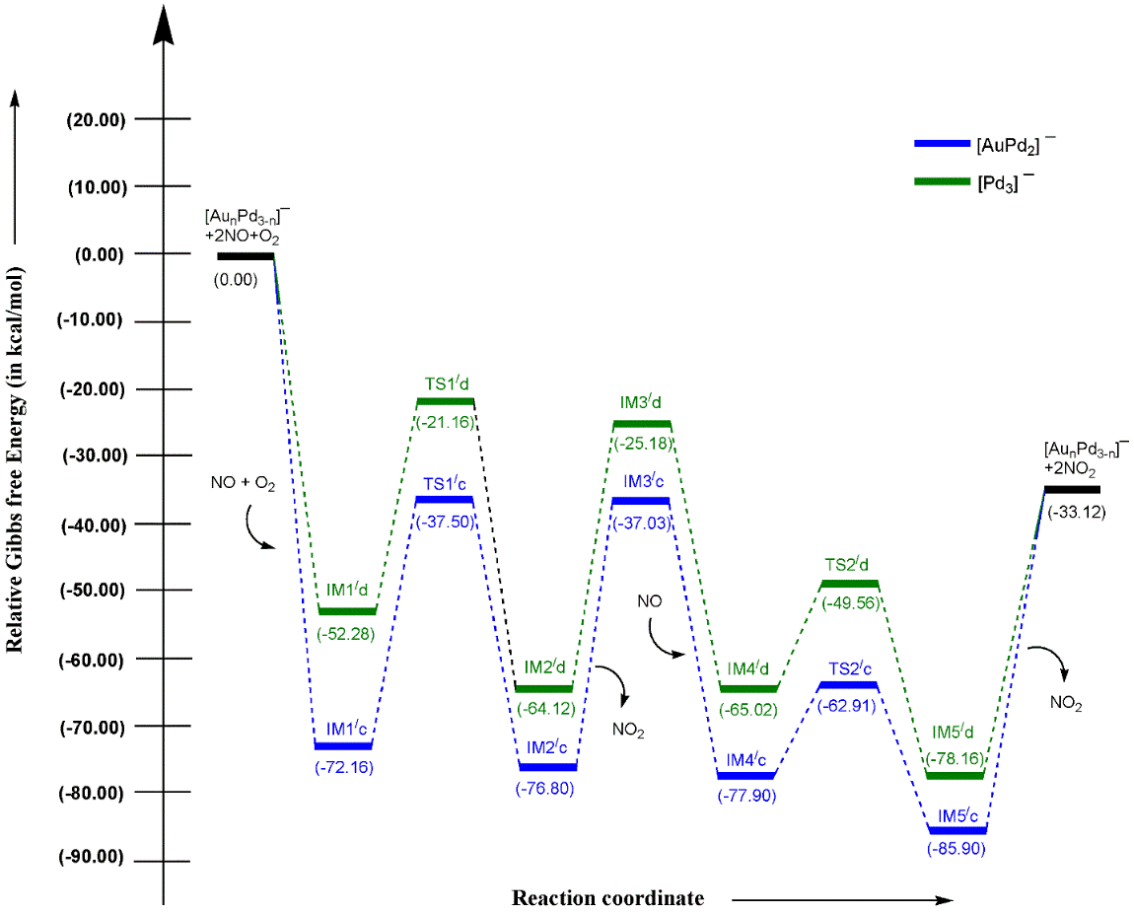

Figure 5.8: Energy profile diagram for LH_{ds} mechanism on $[Au_nPd_{3-n}]^-$ (n=0-3) clusters at M06L/def2TZVP level.

Table 5.8 contains barrier heights (in kcal/mol) for LH_{ss} and LH_{ds} on$[Au_nPd_{3-n}]^-$ (n=0-3) clusters. Looking at the activation barrier, it can be concluded that $[Au_2Pd]^-$cluster is the most efficient catalyst which carries oxidation of NO via LH_{ss} mechanism. The activation barrier for TS1 is lowest (2.43 kcal/mol) for $[Au_2Pd]^-$ owing to the fact that activation of O_2 in IM1b is the highest (d_{O-O}=1.306Å and ν_{O-O}=1119.53 cm^{-1}). For LH_{ss}, TS1 and TS2 represents the formation of first NO_2 while TS3 represents the formation of second NO_2. The barrier height of TS2 is lower for $[AuPd_2]^-$ and $[Pd_3]^-$cluster. Looking at activation barrier of both TS1 and TS2 for LH_{ss}, it is predicted that $[Pd_3]^-$cluster is more proficient in the formation of first NO_2 molecule. However, TS3 possesses higher activation barrier for all the systems, except $[Au_2Pd]^-$ cluster. It is due to the fact that the lone 'O' atom which interacts with NO to form NO_2 molecule, is in bridging position in intermediates IM5a, IM5c and IM5d. It increases the orbital reorganization energy for O atom to

interact with NO. But in case of $[Au_2Pd]^-$ cluster, 'O' atom is adsorbed linearly to Pd site of $[Au_2Pd]^-$, which makes it easier for 'O' atom to interact with NO. Hence, the formation of second NO_2 molecule is more feasible in $[Au_2Pd]^-$ cluster. Comparing barrier heights of TS1, TS2 and TS3 for LH_{ss}, it can be concluded that $[Au_2Pd]^-$ cluster is the more prominent cluster for catalyzing two NO molecules to two NO_2 molecules using LH_{ss} mechanism. In case of LH_{ds} mechanism, TS1/ and TS2/ represents the formation of first NO_2 and second NO_2, respectively. In contrast, the first TS of LH_{ds} bears a high activation barrier for both the $[AuPd_2]^-$ and $[Pd_3]^-$ cluster, making it an ineffective mechanism. It might be explained by the fact that it can be challenging for NO and O_2 to react with each other as both the reactants are adsorbed to the adjacent sites. Hence, we have observed that barrier height decreases when both NO and O_2 are co-adsorbed on the same site. While co-adsorption of reactants at adjacent sites results in higher activation barrier.

Table 5.8: Calculated barrier heights (in kcal/mol) for LH_{ss} and LH_{ds} on $[Au_nPd_{3-n}]^-$ (n=0-3) at M06L/def2TZVP level.

Catalyst	LH_{ss}			LH_{ds}	
	TS1	TS2	TS3	TS1	TS2
$[Au_3]^-$	12.26	15.98	33.73	---	---
$[Au_2Pd]^-$	2.43	15.58	13.13	---	---
$[AuPd_2]^-$	17.43	9.76	37.95	34.66	14.99
$[Pd_3]^-$	4.43	9.90	39.01	31.11	15.46

5.3.4.2 Termolecular Eley Rideal (TER) mechanism

The TER mechanism is a three-molecule reaction process where two pre-adsorbed NO molecules activate the gaseous O_2 molecule. As previously discussed, the co-adsorption of two NO molecules is stronger than co-adsorption of NO and O_2 on all the clusters. Therefore, NO oxidation could possibly occur through the TER mechanism. When two NO molecules co-adsorb at the same atom or at adjacent atoms, two different reaction pathways—TER_{ss} (ss=same site) and TER_{ds}, (ds=same site) respectively—are generated. Figure 5.9 (a), (b) and (c) demonstrate,

respectively, the optimised geometries of intermediates and transition states involved in the catalytic oxidation pathway of NO via TER_{ss} on $[Au_3]^-$, $[AuPd_2]^-$ and $[Pd_3]^-$ clusters while Figure 5.9 (d) represents catalytic oxidation pathway of NO via TER_{ds} on $[Pd_3]^-$ cluster.

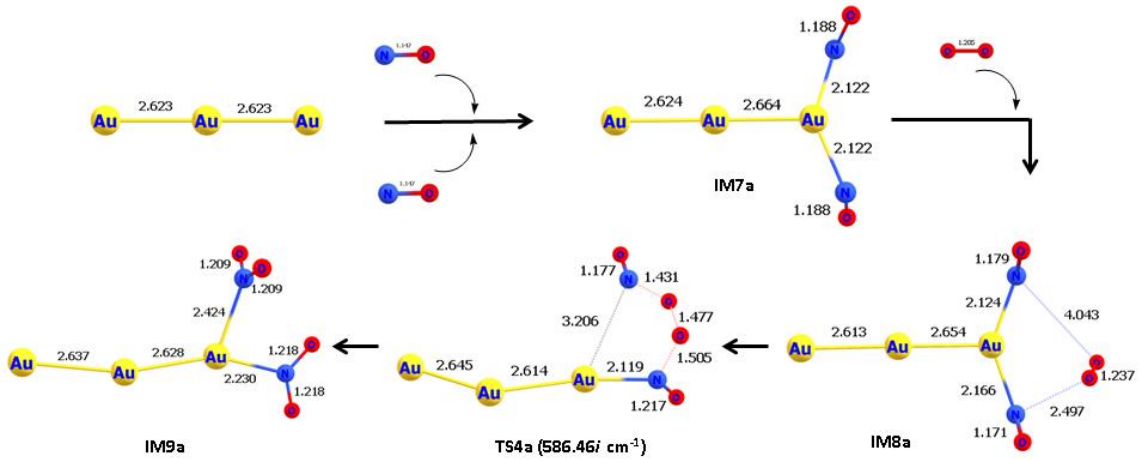

(a)

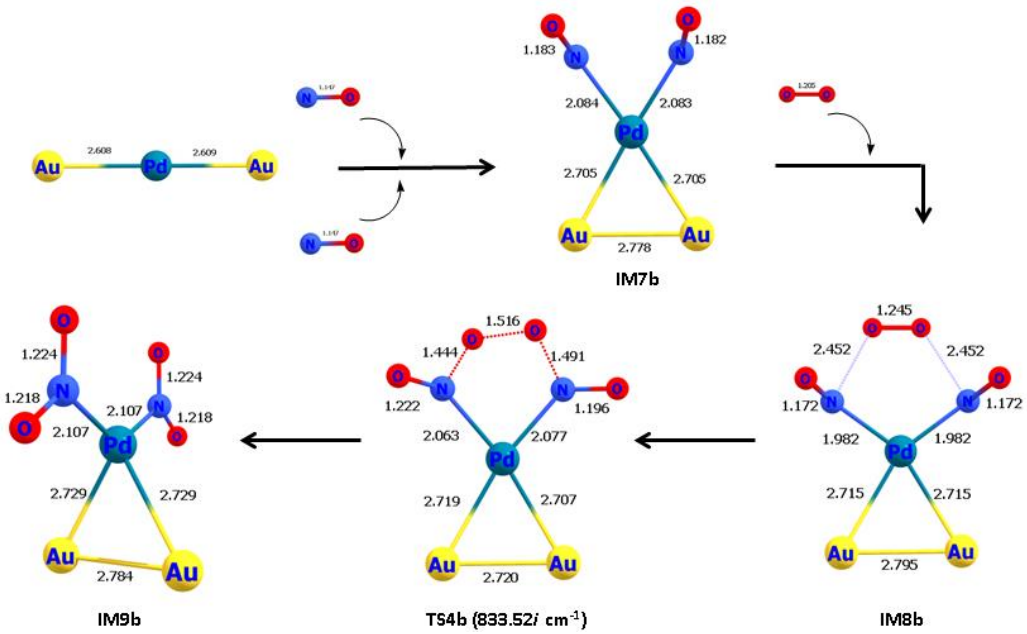

(b)

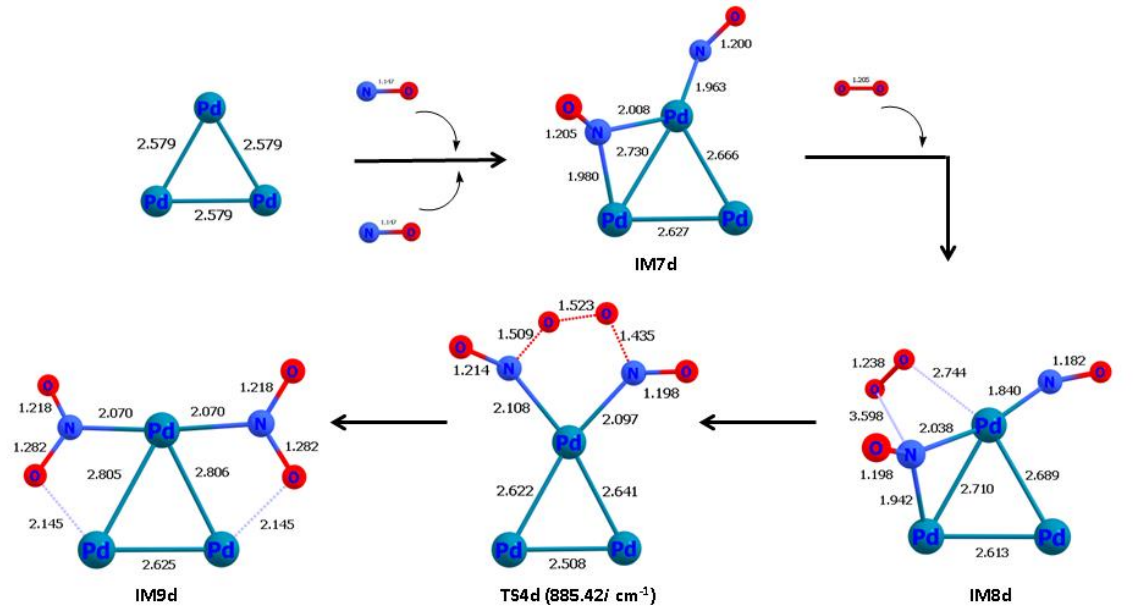

(c)

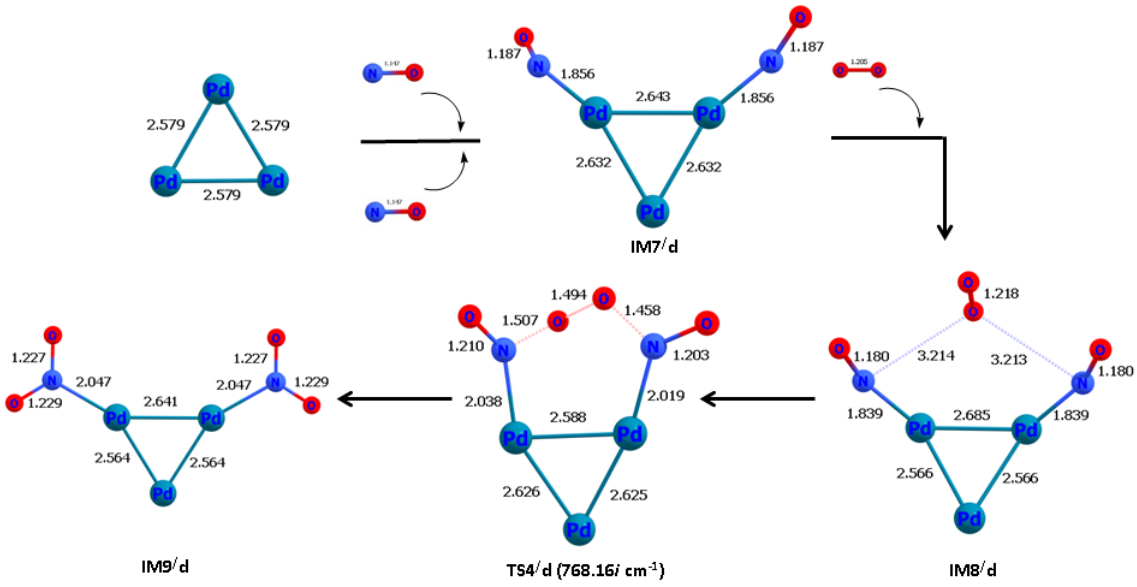

(d)

Figure 5.9: Intermediates and transition states involved in catalytic oxidation pathway of NO via TER_{ss} mechanism on (a) $[Au_3]^-$ (b) $[AuPd_2]^-$ (c) $[Pd_3]^-$ and TER_{ds} on (d) $[Pd_3]^-$ along with their bond lengths (in Å). Imaginary frequency of each TS is given in parentheses.

The reaction mechanism starts when two NO molecules co-adsorbed on the same terminal Au atom of $[Au_3]^-$ cluster, forming IM7a. IM7a is 9.83 kcal/mol lower in energy than the starting material $\{[Au_nPd_{3-n}]^-$ (n=0-3)+ 2NO + $O_2\}$. It is to note that $[Au_3]^-$ cluster follows only TER_{ss} mechanism and not TER_{ds} mechanism. It is

mainly because the distance between two NO molecules increases when they are adsorbed in the terminal Au atoms (Figure 5.9(a)), making it harder for the NO molecules to contain O_2 in gas phase. Bond parameters reveals that both NO molecules are activated in IM7a proportionately (d_{N-O}=1.188Å and ν_{N-O}=1658.54 cm^{-1}). After that, O_2 molecule enters the system and remains at gas phase, leading to the formation of IM8a which is slightly higher in energy (by 4.02 kcal/mol) than that of IM7a. In IM8a, O_2 has modest interaction with that of NO molecules adsorbed to $[Au_3]^-$ cluster. The d_{O-O} and ν_{O-O} in IM8a are 1.237 Å and 1405.59 cm^{-1}, respectively which indicates adequate activation of O_2 which aids the reaction to proceed forward via TER mechanism. Reaction proceeds via TS4a where O_2 interacts with two NO molecules with an activation barrier of 24.43 kcal/mol. Breaking of O-O bond length (1.477 Å) and formation of two new N-O bonds (1.431 Å and 1.505 Å) takes place. Hence, the reaction mechanism ends with the formation of IM9a where two NO_2 molecules are fully formed and attached to $[Au_3]^-$ cluster. This step is thermodynamically feasible as it is exothermic by 43.62 kcal/mol. The energy required for the desorption of two NO molecules from the $[Au_3]^-$ cluster is 16.31 kcal/mol.

IM7b is formed after adsorption of two NO molecules on $[Au_2Pd]^-$cluster which is 41.35 kcal/mol lower in energy than the initial point. Activation of NO takes place in IM7b as evident from its bond length (1.183Å) and vibrational frequency (1719.20 cm^{-1}). The addition of O_2 to IM7b produces IM8b, which is more stable than IM7b by 4.97 kcal/mol. In IM8b, O_2 persists in the gas phase and interacts with two NO molecules at a distance of 2.452 Å. IM8b exhibits little activation of O_2, as revealed from its bond length (1.245 Å) and frequency (1373.56 cm^{-1}).TS4b occurs when O-O bond breaks while interacting with two NO molecules with barrier height of 39.86 kcal/mol. IM9b is formed where two NO_2 molecules are attached to Pd atom of $[Au_2Pd]^-$cluster. This step is also thermodynamically exothermic, however, kinetically not feasible. The desorption energy of two NO_2 molecules to leave $[Au_2Pd]^-$cluster is 43.57 kcal/mol. TER_{ds} is not followed in $[Au_2Pd]^-$ as there is only one active site present in the cluster, i.e Pd site.

TER is not followed in $[AuPd_2]^-$ cluster as O_2 doesn't remain in gas phase and always gets adsorbed on $[AuPd_2]^-$ cluster owing to its higher adsorption energy on

the cluster. For $[Pd_3]^-$ cluster, both TER_{ss} and TER_{ds} is followed. NO molecules co-adsorbing on the same Pd atom give rise to IM7d. In IM7d, one NO molecule is adsorbed linearly while the other NO is adsorbed in a bridging manner. When NO molecules are co-adsorbed adjacently in $[Pd_3]^-$ cluster, it give rise to IM7/d. In PES, the energies of IM7d and IM7/d are 60.83 kcal/mol and 65.30 kcal/mol, respectively lower than the initial point. Inclusion of O_2 in gas phase on IM7d gives IM8d which is 74.19 kcal/mol in energy in PES. The bond length of O_2 in IM8d is 1.238 Å and vibrational frequency is 1394.89 cm^{-1}, thus indicating its activation. While addition of O_2 on IM7/d gives IM8/d which is more stable than IM7/d by 13.41 kcal/mol. Thus, inclusion of O_2 on these pathways are actually favourable. In IM8/d, the bond length of O_2 is 1.218Å and vibrational frequency is 1498.82 cm^{-1}. This indicates that the activation of O_2 happens to be more in case of IM8d than that of IM8/d. This may be attributed to the fact that the distance of O_2 from two NO molecules is far greater (3.214Å and 3.213Å) in IM8/d which makes it difficult to interact. The barrier heights for TS4d and TS4/d are 60.03 kcal/mol and 55.31 kcal/mol, respectively, which makes both the mechanism kinetically unfeasible. Table 5.9 contains activation barrier (in kcal/mol) for TER_{ss} and TER_{ds} on $[Au_nPd_{3-n}]^-$ (n=0-3) clusters at M06L/def2TZVP level. From table 5.9, it can be concluded that TER_{ss} mechanism is more feasible for catalytic oxidation of two NO molecules to two NO_2 molecules on $[Au_3]^-$ cluster while other clusters are kinetically unfavorable for catalyzing oxidation of NO using TER mechanism. Figure 5.10 includes PES for both TER_{ss} and TER_{ds} mechanism on $[Au_nPd_{3-n}]^-$ (n=0-3) clusters at M06L/def2TZVP level.

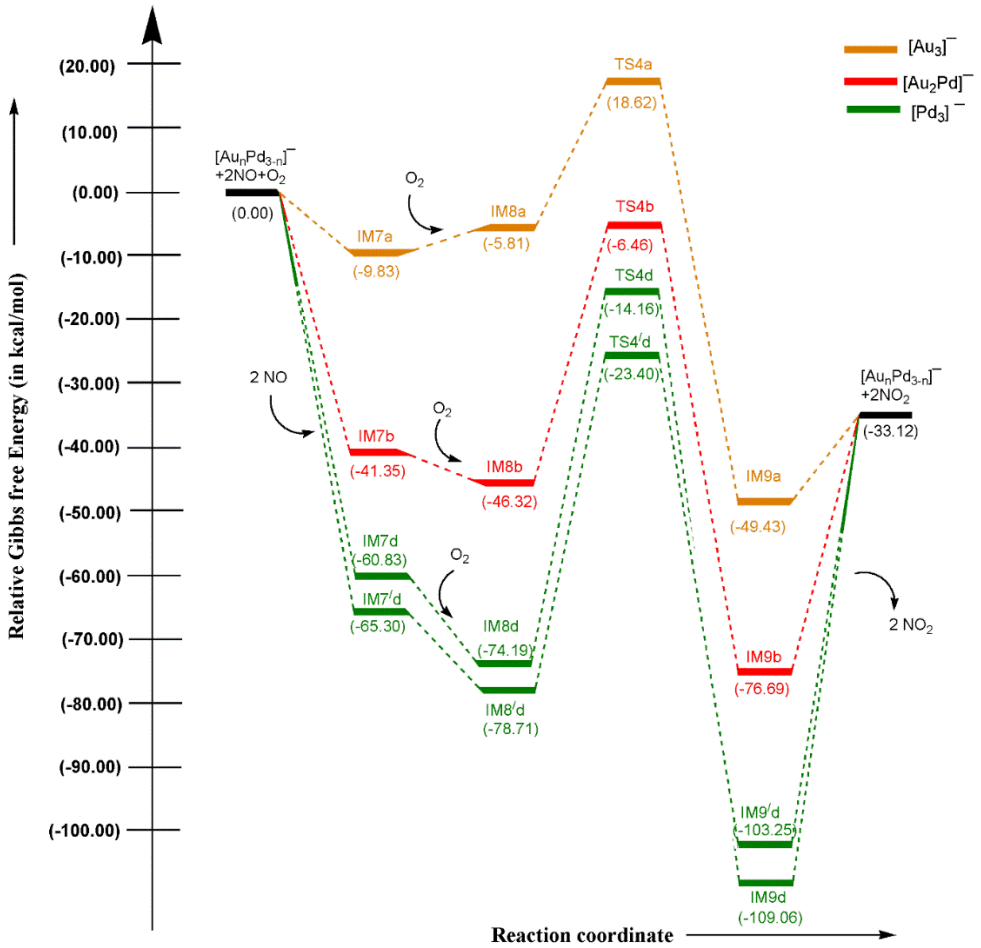

Figure 5.10: Energy profile diagram for both TER_{ss} and TER_{ds} mechanism on $[Au_nPd_{3-n}]^-$ (n=0-3) clusters at M06L/def2TZVP level.

Table 5.9: Activation barrier (in kcal/mol) for TER_{ss} and TER_{ds} on {$[Au_nPd_{3-n}]^-$ (n=0-3)clusters at M06L/def2TZVP level.

Catalyst	Activation barrier (in kcal/mol)	
	TER_{ss}	TER_{ds}
	TS4	TS4/
$[Au_3]^-$	24.43	---
$[Au_2Pd]^-$	39.86	---
$[Pd_3]^-$	60.03	55.31

5.3.4.3 Termolecular Langmuir Hinshelwood (TLH) mechanism

Another three-molecule reaction process is the termolecular Langmuir Hinshelwood (TLH) mechanism, in which two NO molecules and one O_2 molecule co-adsorb onto the catalyst to interact with one another. TLH mechanism has been followed in all the clusters, except $[Au_3]^-$. Co-adsorption of three molecules (two NO and one O_2) on the same site gives rise to TLH_{ss} (ss=same site) while co-adsorption at different sites give rise to TLH_{ds} (ds=different sites).

IM10b is formed when two NO molecules co-adsorb onto the Pd atom of the $[Au_2Pd]^-$ cluster. This intermediate has an energy that is 39.65 kcal/mol lower than the starting point. When an O_2 molecule is added to IM10b, IM11b is formed, which is 10 kcal/mol more stable than IM10b. After adsorption on the cluster, the O_2 molecule becomes sufficiently active to carry out the process. The same is revealed by the bond lengths of O_2 (1.254 Å) and ν_{O-O} (1341.01 cm^{-1}) in IM11b. The O atom of O_2 connects with one of the NO molecules in TS5b. This process has an activation barrier of 8.10 kcal/mol and is mildly endothermic (1.96 kcal/mol) in terms of energy. Reaction proceeds via TS6b where the free O atom of O-O-N-O species interacts with another NO atom, forming O-N-O-O-N-O species, which leads to the cleaving of O-O bond. This step occurs with an activation barrier of 21.81 kcal/mol. Eventually, IM13b forms, containing two NO_2 molecules that departs the system with a desorption energy of 64.88 kcal/mol.

Both TLH_{ss} and TLH_{ds} is followed in case of $[AuPd_2]^-$cluster. In TLH_{ss}, the co-adsorption of two NO molecules onto the one Pd atom of $[AuPd_2]^-$cluster results in the formation of IM7c. In IM7c, one NO molecule is adsorbed in a linear fashion while the other is adsorbed in a bridging form, with N atom of NO forming bonds with both the Pd atoms of $[AuPd_2]^-$ cluster. Energy-wise, this intermediate is 84.70 kcal/mol in PES. IM8c is formed after the addition of O_2 molecule which gets adsorbed in between the two NO molecules. It is observed that the O_2 molecule is suitably activated {d_{O-O} (1.260 Å) and ν_{O-O} (1324.07 cm^{-1})} which makes the reaction to proceed forward. TLH_{ss} undergoes via one step where O_2 molecule interacts with both the NO molecules simultaneously in TS5c, forming O-N-O-O-N-O species. Looking at TS5c, it is evident that O-O bond is breaking (1.518Å) and new N-O bonds are formed (1.489Å and 1.452Å). The barrier height of this step is 52.42

kcal/mol which makes it kinetically unfavorable. In case of TLH_{ds}, the co-adsorption of two NO molecules onto different Pd atoms of $[AuPd_2]^-$cluster yields IM7/c which is energetically almost similar to IM7c. IM8/c is formed upon inclusion of O_2. It is to note that activation of O_2 is more ({d_{O-O} (1.275 Å) and ν_{O-O} (1213.55 cm^{-1})} in IM8/c in comparison to that of IM8c. This may facilitates the reaction as evident from the lower energy barrier height of TS5/c (31.16 kcal/mol) as compared toTS5c (52.42 kcal/mol). Two NO_2 molecules are formed in IM9/c which is the most stable intermediate in PES. This is also the reason for higher desorption energies of two NO_2 molecules (87.79 kcal/mol) on $[AuPd_2]^-$cluster leaving via TLH_{ds} mechanism.

Similar scenario occurs in $[Pd_3]^-$ cluster where it follows both TLH_{ss} and TLH_{ds} mechanism. IM7d is formed in TLH_{ss} when two NO molecules co-adsorb onto the single Pd atom of the $[Pd_3]^-$ cluster. The co-adsorption manner of two NO molecules in IM7d is similar to that of IM7c. Addition of O_2 yields IM8d which is more stable (-76.30 kcal/mol) than that of IM7d (-73.25 kcal/mol) in PES. TLH_{ss} in $[Pd_3]^-$ cluster undergoes via two transition states i.e.TS5d and TS6d. In TS5d, O atom of O_2 interacts with one of the NO, forming O-N-O-O species via activation barrier of 12.19 kcal/mol. In TS6d, another NO attacks the free O atom of O-N-O-O species, forming O-N-O-O-N-O species, which facilitates the breaking of O-O bond. The barrier height for TS6d is 40.28 kcal/mol. The second step is highly exothermic (by 72.95 kcal/mol) but kinetically not favorable. TLH_{ds} mechanism is followed when two NO molecules co-adsorb onto the different Pd atoms of $[Pd_3]^-$ cluster, forming intermediate IM7/d. Reaction proceed via IM8/d which is slightly stable than IM7/d by 1.13 kcal/mol. TLH_{ds} mechanism on $[Pd_3]^-$ cluster undergoes via one transition state (TS5/d) which has an activation barrier of 45.97 kcal/mol. Generally, O_2 is positioned in between two NO molecules so that it becomes easier for it to form O-N-O-O-N-O species. However, in IM8/d, O_2 is positioned outwards and not in between the two molecules. Hence, a greater orbital reorganization energy is required for O_2 in TS5/d to form O-N-O-O-N-O species. Figure 5.11 and Figure 5.12 includes intermediates and transition states involved in catalytic oxidation pathway of NO via TLH_{ss} and TLH_{ds} mechanism, respectively. Figure 5.13 represents PES for both TLH_{ss} and TLH_{ds} mechanism at M06L/def2TZVP level. One important thing to be observed is that the spin is conserved for all the reaction pathways.

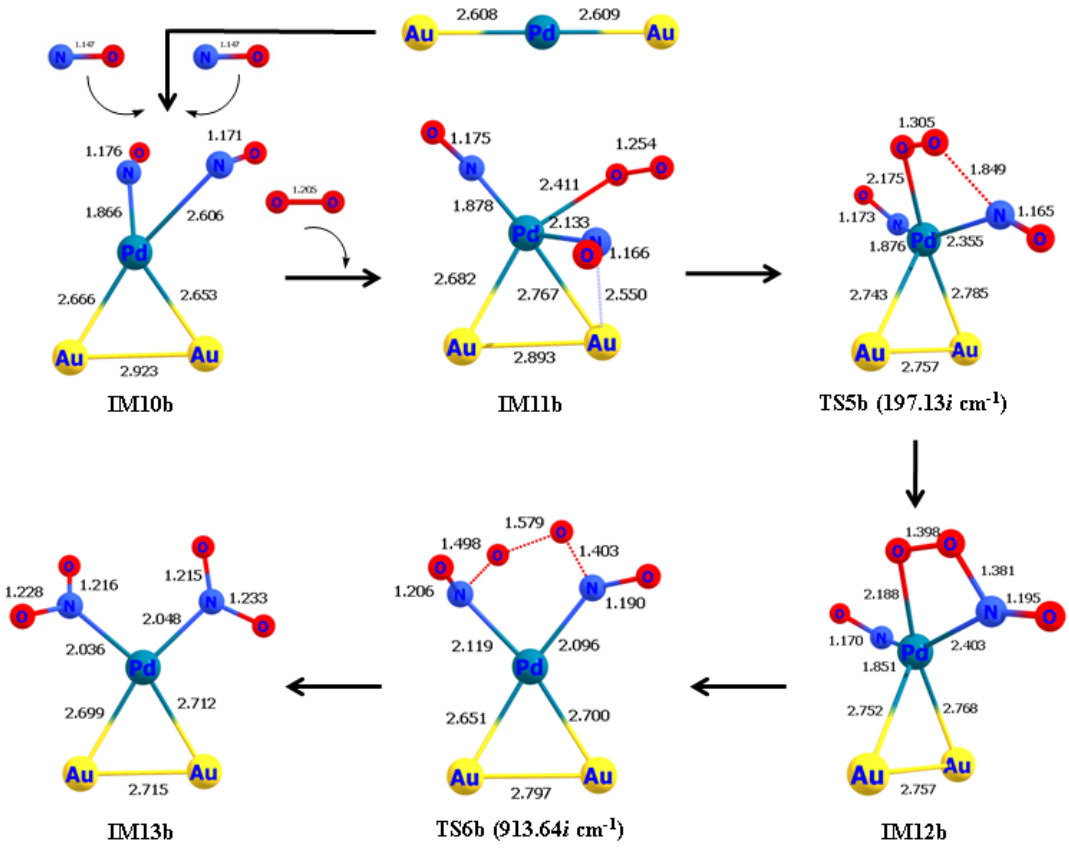
IM10b
IM11b
TS5b (197.13*i* cm^{-1})
IM12b
TS6b (913.64*i* cm^{-1})
IM13b

(a)

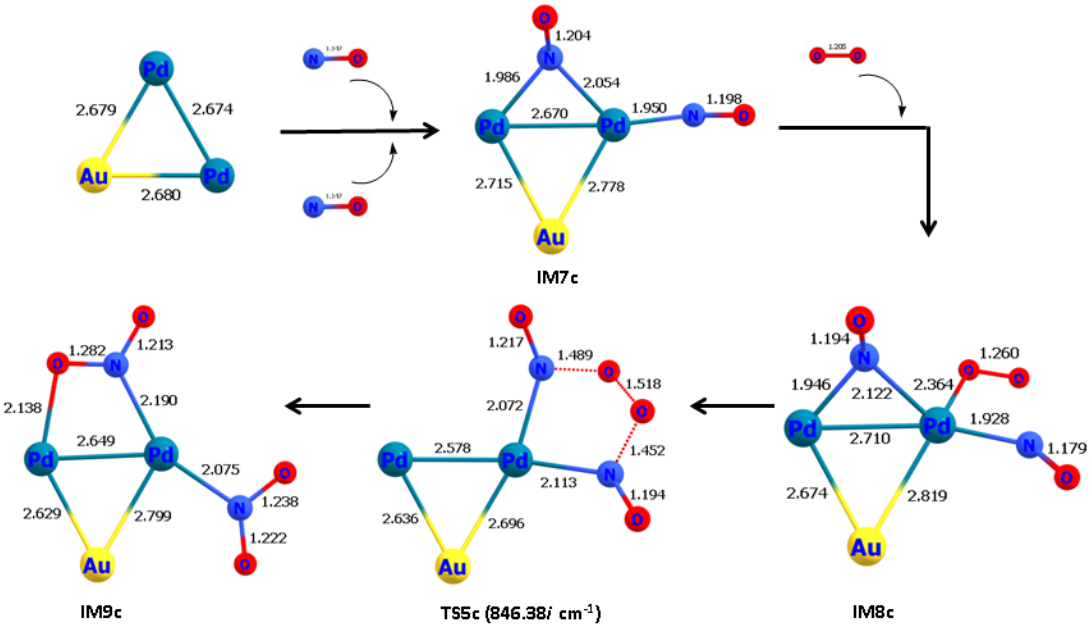
IM7c
IM8c
TS5c (846.38*i* cm^{-1})
IM9c

(b)

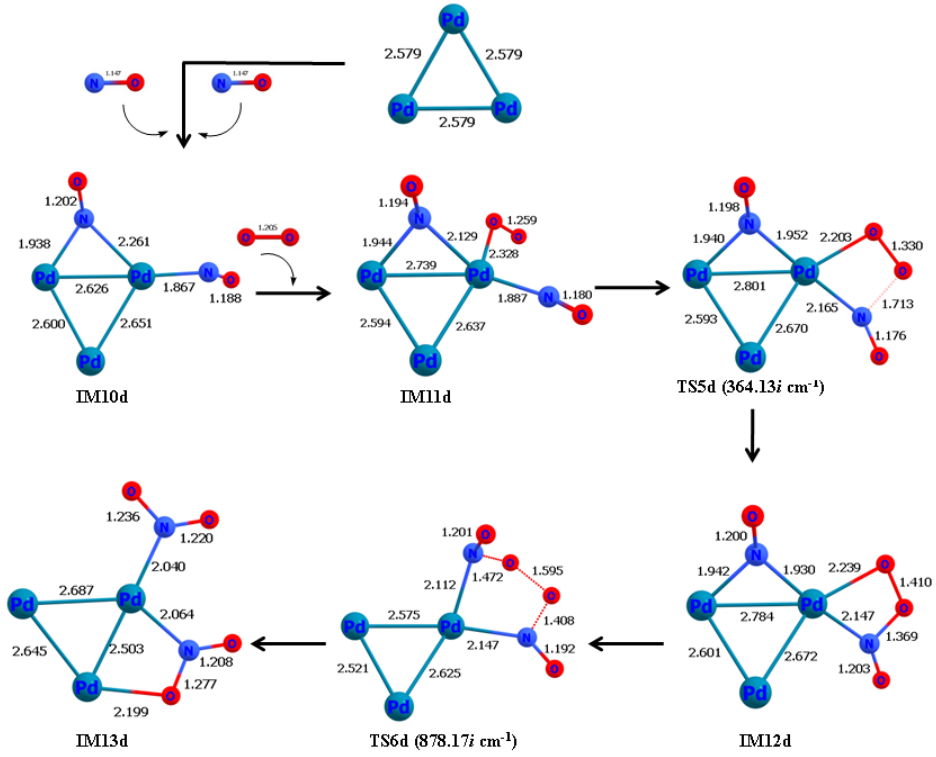

(c)

Figure 5.11: Intermediates and transition states involved in catalytic oxidation pathway of NO via TLH_{ss} mechanism on (a) $[Au_2Pd]^-$ (b) $[AuPd_2]^-$ and (c) $[Pd_3]^-$along with their bond lengths (in Å). Imaginary frequency of each TS is given in parentheses.

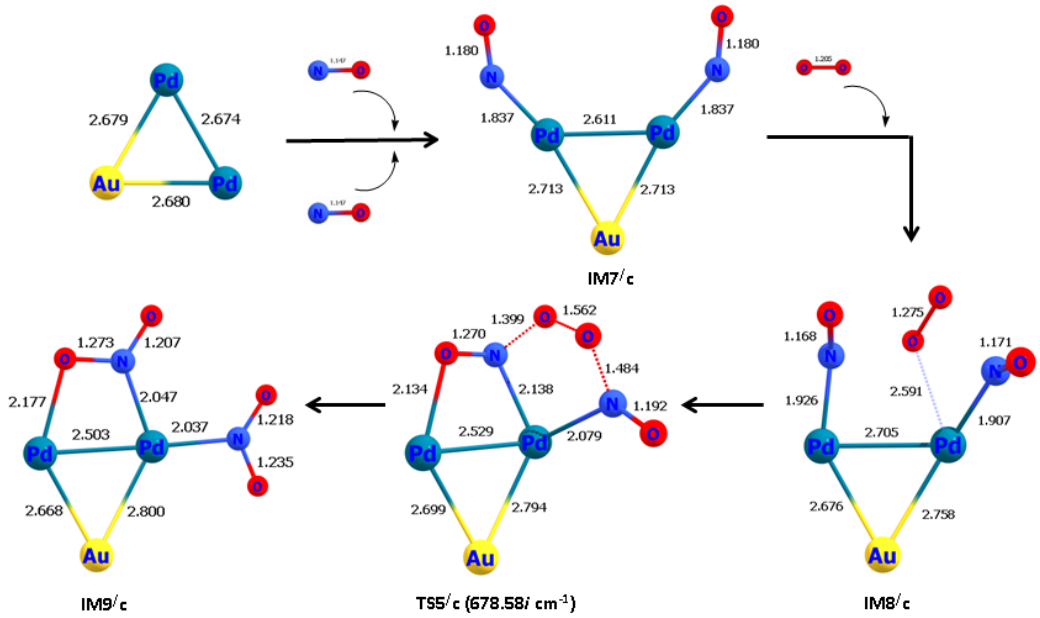

(a)

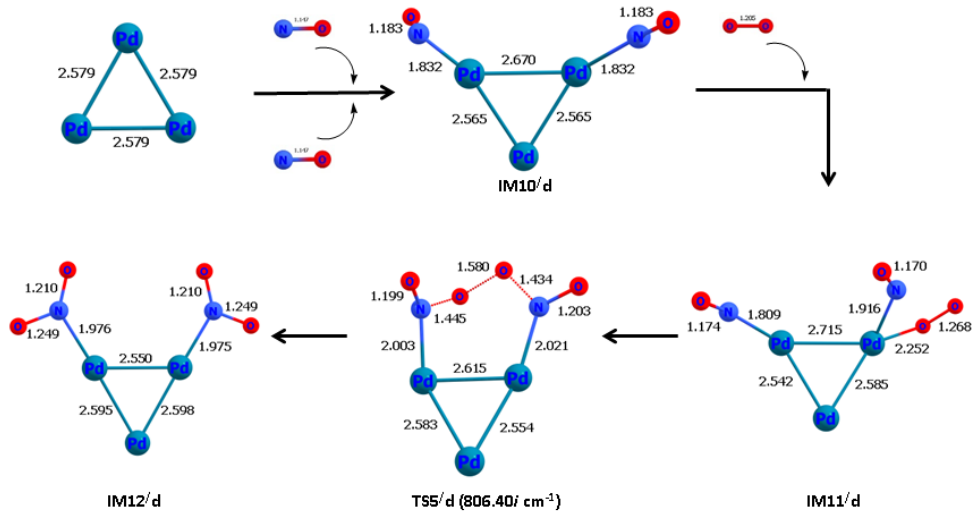

(b)

Figure 5.12: Intermediates and transition states involved in catalytic oxidation pathway of NO via TLH_{ds} mechanism on (a) $[AuPd_2]^-$ and (b) $[Pd_3]^-$along with their bond lengths (in Å). Imaginary frequency of each TS is given in parentheses.

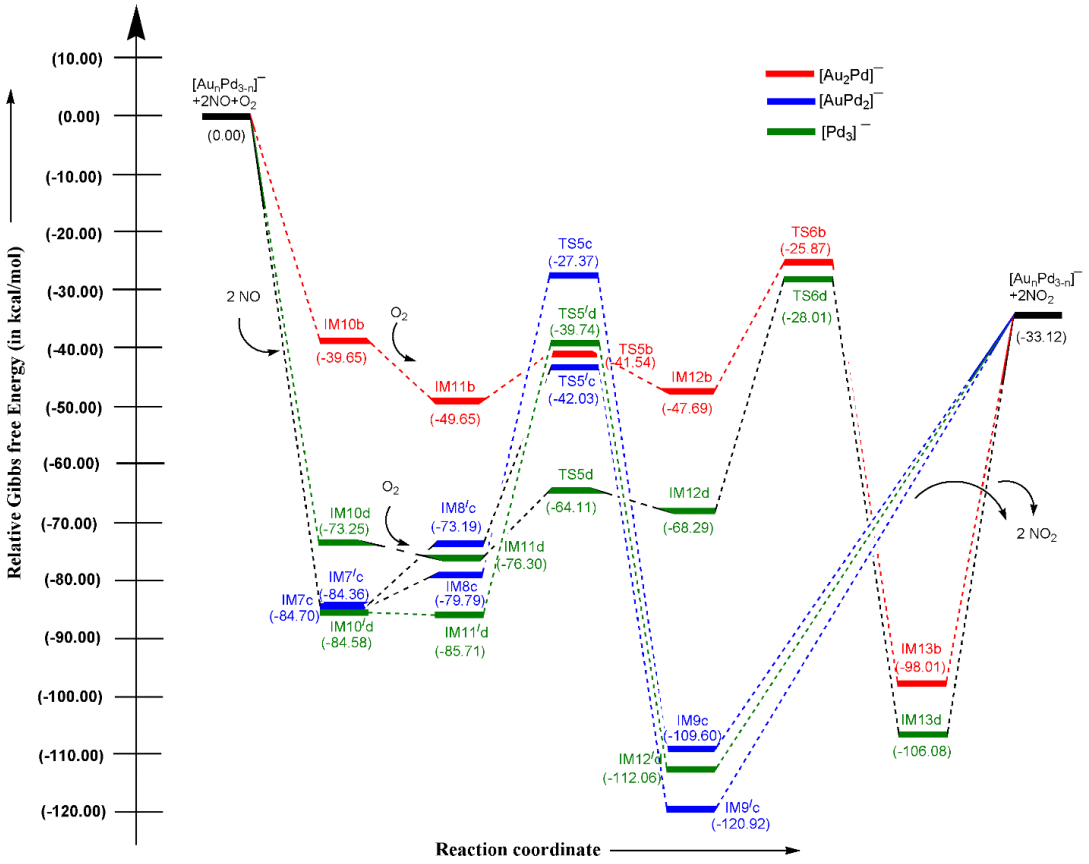

Figure 5.13: Energy profile diagram for both TLH_{ss} and TLH_{ds} mechanism on $[Au_nPd_{3-n}]^-$ (n=0-3) clusters at M06L/def2TZVP level.

Table 5.10: Activation barrier (in kcal/mol) for TLH_{ss} and TLH_{ds} on $[Au_nPd_{3-n}]^-$ (n=0-3) clusters at M06L/def2TZVP level.

Catalyst	Activation barrier (in kcal/mol)		
	TLH_{ss}		TLH_{ds}
	TS5	TS6	TS5/
$[Au_2Pd]^-$	8.10	21.81	---
$[AuPd_2]^-$	52.42	---	31.16
$[Pd_3]^-$	12.19	40.28	45.97

5.3.4.4 Efficiency of clusters using energetic span model

The efficiency of a catalyst from a free energy reaction pathway has been examined using the energetic span model. To determine the efficiency of the catalytic processes, the value of the energetic span (δE) is computed using Equation (5) and presented in Table 5.11. Comparing LH_{ss} and LH_{ds} mechanism, δE value is found to be lowest (21.68 kcal/mol) for $[Au_2Pd]^-$ cluster in which TS2b and IM6b are TDTS and TDI, respectively. Whereas IM3a corresponds to TS3a have a maximum value δE value of 43.52 kcal/mol for NO catalytic oxidation reaction on $[Au_3]^-$ cluster. Hence, $[Au_2Pd]^-$ cluster will have a higher turnover frequency (TOF) via LH_{ss} mechanism while $[Au_3]^-$ will have a lower TOF. Looking at TER mechanism, $[Au_3]^-$ cluster has a lower δE value of 34.93 kcal/mol in which TS4a and IM9a are TDTS and TDI, respectively. This means $[Au_3]^-$ can effectively catalyze oxidation of 2 NO to 2 NO_2 via TER_{ss} mechanism. While $[Au_2Pd]^-$ is the most effective when it comes to TLH mechanism where IM13b corresponds to TS6b have a δE value of 39.02 kcal/mol.

Overall, the lowest δE value comes from $[Au_2Pd]^-$ cluster when it follows LH_{ss} mechanism. Comparatively, $[Au_2Pd]^-$ cluster is the most efficient cluster which can catalyze two NO molecules to two NO_2 molecules using LH_{ss} mechanism.

Table 5.11: Values of key state energies (in kcal/mol), δE value (in kcal/mol) and TOF (in s^{-1}) for $[Au_nPd_{3-n}]^-$ (n=0-3) clusters

	LH_{ss}				**LH_{ds}**			
Clusters	TDTS	TDI	δ_E	TOF	TDTS	TDI	δ_E	TOF
$[Au_3]^-$	-1.04(TS3a)	-44.56(IM3a)	43.52	6.94×10^{-20}	---	---	---	---
$[Au_2Pd]^-$	-13.93(TS2b)	-68.73(IM6b)	21.68	7.51×10^{-04}	---	---	---	---
$[AuPd_2]^-$	-51.36(TS3c)	-89.32(IM5c)	37.96	8.38×10^{-16}	-37.50(TS1/c)	-72.16(IM1/c)	34.66	2.22×10^{-13}
$[Pd_3]^-$	-49.84(TS3d)	-88.85(IM5d)	39.01	1.42×10^{-16}	-21.16(TS1/d)	-52.28 IM1/d)	31.12	8.81×10^{-11}
	TER_{ss}				**TER_{ds}**			
	TDTS	TDI	δ_E	TOF	TDTS	TDI	δ_E	TOF
$[Au_3]^-$	18.62(TS4a)	-49.43(IM9a)	34.93	1.41×10^{-13}	---	---	---	---
$[Au_2Pd]^-$	-6.46(TS4b)	-46.32(IM8b)	39.86	3.38×10^{-17}	---	---	---	---
$[Pd_3]^-$	-14.16(TS4d)	-109.06(IM9d)	61.78	2.72×10^{-33}	-23..40(TS4/d)	-78.71(IM8/d)	55.31	1.53×10^{-28}
	TLH_{ss}				**TLH_{ds}**			
	TDTS	TDI	δ_E	TOF	TDTS	TDI	δ_E	TOF
$[Au_2Pd]^-$	-25.87(TS6b)	-98.01(IM13b)	39.02	1.40×10^{-16}	---	---	---	
$[AuPd_2]^-$	-27.37(TS5c)	-84.70(IM7c)	57.33	5.04×10^{-30}	-42.03(TS5/c)	-120.92(IM9/c)	45.77	1.55×10^{-21}
$[Pd_3]^-$	-28.01(TS6d)	-76.30(IM8d)	48.29	2.18×10^{-23}	-39.74(TS5/d)	-85.71(IM8/d)	45.97	1.10×10^{-21}

The TOF values for NO oxidation generally depends upon specific catalytic material, reaction conditions (temperature and pressure), feed composition (concentration of NO, O_2, NO_2) etc. In our work, we have reported TOF of our most efficient Langmuir Hinshelwood (LH) mechanism in the range 10^{-4} s^{-1} at 298 K. This value is reasonable with the work done by Narula and his group [82] where NO oxidation was performed on single supported Pt atoms in which TOF values were reported to be (1.8-10) $\times10^{-4}$ s^{-1} in temperature range of 538K-688K. It is expected that our TOF may increase with the increase in temperature.

Nevertheless, some of the literatures have reported higher TOFs under different conditions. Smeltz et al [83] reported high TOF of 0.34 s^{-1} at 573 K for NO oxidation on Pt (111) where feed composition was 73 ppm NO, 27 ppm NO_2 and 5% O_2. Mulla et al. [84] reported 3.5 * 10^{-3} s^{-1} at 573K at different feed composition. Even more striking, NO oxidation on IrO_2 (110) [85] has been shown to proceed with a TOF as high as 37 s^{-1} which is quite efficient.

Although our TOF values are low in comparison to others, our main aim was not to maximize absolute activity, but rather provide a clear DFT based insights into different mechanistic pathways and to choose the most efficient path for NO oxidation on our chosen monometallic and bimetallic systems. Looking at TOF values comparatively tells that bimetallic system are more efficient.

5.4 Significant Outcomes

In this work, we systematically studied the adsorption characteristics of NO and $O_2$and reaction mechanism of oxidation of two NO molecules to two NO_2 molecules on $[Au_nPd_{3-n}]^-$(n=0-3) clusters.

1. Adsorption energy analysis revealed that on adding Pd atom to a pure $[Au_3]^-$ cluster, the adsorption energy of both NO and O_2 increases.
2. Moreover, it is also observed that reactants prefer to bind to Pd site of bimetallic $[Au_2Pd]^-$ and $[AuPd_2]^-$ clusters.
3. Results further advocates that compared to NO and O_2 and two O_2 molecules, the co-adsorption energy values of two NO molecules on the catalyst are more negative.
4. Based on the co-adsorption energies of the reactants on $[Au_nPd_{3-n}]^-$(n=0-3) clusters, the detailed reaction path under L-H, TER and TLH mechanism were investigated.
5. Based on the different configuration possible for the co-adsorption, mechanisms are distinguished into LH_{ss} (same site), LH_{ds} (different site), TER_{ss}, TER_{ds}, TLH_{ss} and TLH_{ds}. The comparison of barrier heights reveals that LH_{ss} is the most proficient pathway which can catalyze two NO to NO_2 molecules using molecular O_2 on $[Au_2Pd]^-$ cluster.

6. Based on the energetic span model calculation, $[Au_2Pd]^-$ is the most efficient catalyst since it has the lowest δE value and the highest TOF value. Hence, it has been concluded that Pd alloying on pure $[Au_3]^-$ cluster increases its reactivity.

5.5 Bibliography

[1] Liu, S. W., Guo, R. T., Sun, X., Liu, J., Pan, W. G., Shi, X., Wang, Z. Y., Liu, X. Y., and Qin, H. Selective catalytic reduction of NO_x over $Ce/TiZrO_x$ catalyst: The promoted K resistance by $TiZrO_x$ support. *Molecular Catalysis*, 462:19-27, 2019.

[2] Gao, Z., Liu, X., Li, A., Li, X., Ding, X., and Yang, W. Bimetallic sites supported on N-doped graphene ((Fe, Co)/N-GN) as a new catalyst for NO oxidation: A theoretical investigation. *Molecular Catalysis*, 470:56-66, 2019.

[3] Najjar, Y. S. Gaseous pollutants formation and their harmful effects on health and environment. *Innovative energy policies*, 1:1-9, 2011.

[4] Wang, J., Zhao, H., Haller, G., and Li, Y. Recent advances in the selective catalytic reduction of NO_x with NH_3 on Cu-Chabazite catalysts. *Applied Catalysis B: Environmental*, 202:346-354, 2017.

[5] Chen, Z., Wang, F., Li, H., Yang, Q., Wang, L. and Li, X. Low-temperature selective catalytic reduction of NO_x with NH_3 over Fe–Mn mixed-oxide catalysts containing $Fe_3Mn_3O_8$ phase. *Industrial & engineering chemistry research*, 51:202-212, 2012.

[6] Forzatti, P., Castoldi, L., Nova, I., Lietti, L., and Tronconi, E. NO_x removal catalysis under lean conditions. *Catalysis today*, 117:316-320, 2006.

[7] Madia, G., Koebel, M., Elsener, M., and Wokaun, A. The effect of an oxidation precatalyst on the NO_x reduction by ammonia SCR. *Industrial & engineering chemistry research*, 41:3512-3517, 2002.

[8] Jõgi, I., Erme, K., Raud, J., and Laan, M. Oxidation of NO by ozone in the presence of TiO_2 catalyst. *Fuel*, 173:45-51, 2016.

[9] Shao, J., Yang, Y., Whiddon, R., Wang, Z., Lin, F., He, Y., Kumar, S., and Cen, K. Investigation of NO removal with ozone deep oxidation in Na_2CO_3 solution. *Energy & Fuels*, 33:4454-4461, 2019.

[10] Yang, W., Chen, L., Zhou, B., Jia, Z., Liu, X., Liu, Y., Li, H., and Gao, Z. NO oxidation using H_2O_2 at a single-atom iron catalyst. *The Journal of Physical Chemistry C*, 127:13011-13020, 2023.

[11] Xue, Z., Du, X., Rac, V., Rakic, V., Wang, X., Chen, Y., Xiang, J., and Song, L. Partial oxidation of NO by H_2O_2 and afterward reduction by NH_3-selective catalytic reduction: an efficient method for NO removal. *Industrial & Engineering Chemistry Research*, 59:9393-9397, 2020.

[12] Fang, P., Cen, C. P., Wang, X. M., Tang, Z. J., Tang, Z. X., and Chen, D. S. Simultaneous removal of SO_2, NO and Hg^0 by wet scrubbing using urea+ $KMnO_4$ solution. *Fuel Processing Technology*, 106:645-653, 2013.

[13] Hong, Z., Wang, Z., and Li, X. Catalytic oxidation of nitric oxide (NO) over different catalysts: an overview. *Catalysis Science & Technology*, 7:3440-3452, 2017.

[14] Pattrick, G., Van der Lingen, E., Corti, C. W., Holliday, R. J., and Thompson, D. T. The potential for use of gold in automotive pollution control technologies: a short review. *Topics in catalysis*, 30:273-279, 2004.

[15] Ueda, A. and Haruta, M. Nitric oxide reduction with hydrogen, carbon monoxide, and hydrocarbons over gold catalysts. *Gold Bulletin*, 32:3-11, 1999.

[16] Ueda, A. and Haruta, M. Reduction of nitrogen monoxide with propene over Au/Al_2O_3 mixed mechanically with Mn_2O_3. *Applied Catalysis B: Environmental*, 18:115-121, 1998.

[17] Zhang, Y., Cattrall, R. W., McKelvie, I. D., and Kolev, S. D. Gold, an alternative to platinum group metals in automobile catalytic converters. *Gold Bulletin*, 44:145-153, 2011.

[18] Panayotov, D. A. and Morris, J. R. Surface chemistry of Au/TiO_2: Thermally and photolytically activated reactions. *Surface Science Reports*, 71:77-271, 2016.

[19] Wang, X., Wang, A., Wang, X., Yang, X., and Zhang, T. Selective catalytic reduction of NO with propene over $Au/CeO_2/Al_2O_3$ catalysts. *Gold Bulletin*, 40:52-58, 2007.

[20] Pattrick, G., Van der Lingen, E., Corti, C. W., Holliday, R. J., and Thompson, D. T. The potential for use of gold in automotive pollution control technologies: a short review. *Topics in catalysis*, 30:273-279, 2004.

[21] Xu, C., Su, J., Xu, X., Liu, P., Zhao, H., Tian, F., and Ding, Y. Low temperature CO oxidation over unsupported nanoporous gold. *Journal of the American Chemical Society*, 129:42-43, 2007.

[22] Hagen, J., Socaciu, L. D., Elijazyfer, M., Heiz, U., Bernhardt, T. M., and Wöste, L. Coadsorption of CO and O_2 on small free gold cluster anions at cryogenic temperatures: Model complexes for catalytic CO oxidation. *Physical Chemistry Chemical Physics*, 4:1707-1709, 2002.

[23] Hayashi, T., Tanaka, K., and Haruta, M. Selective vapor-phase epoxidation of propylene over Au/TiO_2 catalysts in the presence of oxygen and hydrogen. *Journal of Catalysis*, 178:566-575, 1998.

[24] Zalc, J. M., Sokolovskii, V., and Löffler, D. G. Are noble metal-based water–gas shift catalysts practical for automotive fuel processing? *Journal of Catalysis*, 206:169-171, 2002.

[25] Liu, Z. P., Jenkins, S. J., and King, D. A. Origin and activity of oxidized gold in water-gas-shift catalysis. *Physical Review Letters*, 94:196102, 2005.

[26] Boronat, M., Leyva-Pérez, A., and Corma, A. Theoretical and experimental insights into the origin of the catalytic activity of subnanometric gold clusters: attempts to predict reactivity with clusters and nanoparticles of gold. *Accounts of chemical research*, 47:834-844, 2014.

[27] Tyo, E. C. and Vajda, S. Catalysis by clusters with precise numbers of atoms. *Nature nanotechnology*, 10:577-588, 2015.

[28] Liu, L. and Corma, A. Metal catalysts for heterogeneous catalysis: from single atoms to nanoclusters and nanoparticles. *Chemical reviews*, 118:4981-5079, 2018.

[29] Qiao, B., Wang, A., Yang, X., Allard, L. F., Jiang, Z., Cui, Y., Liu, J., Li, J., and Zhang, T. Single-atom catalysis of CO oxidation using Pt_1/FeO_x. *Nature chemistry*, 3:634-641, 2011.

[30] Zhang, J., Deng, Y., Cai, X., Chen, Y., Peng, M., Jia, Z., Jiang, Z., Ren, P., Yao, S., Xie, J. and Xiao, D. Tin-assisted fully exposed platinum clusters stabilized on

defect-rich graphene for dehydrogenation reaction. *Acs Catalysis*, 9:5998-6005, 2019.

[31] Xu, C., Su, J., Xu, X., Liu, P., Zhao, H., Tian, F., and Ding, Y. Low temperature CO oxidation over unsupported nanoporous gold. *Journal of the American Chemical Society*, 129:42-43, 2007.

[32] Mikami, Y., Dhakshinamoorthy, A., Alvaro, M., and Garcia, H. Catalytic activity of unsupported gold nanoparticles. *Catalysis Science & Technology*, 3:58-69, 2013.

[33] Sanchez, A., Abbet, S., Heiz, U., Schneider, W.D., Häkkinen, H., Barnett, R.N. and Landman, U. When gold is not noble: nanoscale gold catalysts. *The Journal of Physical Chemistry A*, 103:9573-9578, 1999.

[34] Wallace, W. T. and Whetten, R. L. Coadsorption of CO and O_2 on selected gold clusters: evidence for efficient room-temperature CO_2 generation. *Journal of the American Chemical Society*, 124:7499-7505, 2002.

[35] Cox, D. M., Brickman, R., Creegan, K., and Kaldor, A. Gold clusters: reactions and deuterium uptake. *Zeitschrift für Physik D Atoms, Molecules and Clusters*, 19:353-355, 1991.

[36] Huang, W., Zhai, H. J., and Wang, L. S. Probing the Interactions of O_2 with Small Gold Cluster Anions (Au_n^-, n= 1– 7): Chemisorption vs Physisorption. *Journal of the American Chemical Society*, 132:4344-4351, 2010.

[37] Woodham, A., Meijer, G., and Fielicke, A. Activation of molecular oxygen by anionic gold clusters. *Angewandte Chemie International Edition*, 51:4444-4447, 2012.

[38] Pal, R., Wang, L. M., Pei, Y., Wang, L. S., and Zeng, X. C. Unraveling the mechanisms of O_2 activation by size-selected gold clusters: transition from superoxo to peroxo chemisorption. *Journal of the American Chemical Society*, 134:9438-9445, 2012.

[39] Sun, Q., Jena, P., Kim, Y. D., Fischer, M., and Ganteför, G. Interactions of Au cluster anions with oxygen. *The Journal of chemical physics*, 120:6510-6515, 2004.

[40] Citra, A., Wang, X., and Andrews, L. Reactions of laser-ablated gold with nitric oxide: infrared spectra and DFT calculations of AuNO and Au $(NO)_2$ in solid Argon and Neon. *The Journal of Physical Chemistry A*, 106:3287-3293, 2002.

[41] Ding, X., Li, Z., Yang, J., Hou, J. G., and Zhu, Q. Theoretical study of nitric oxide adsorption on Au clusters. *The Journal of chemical physics*, 121:2558-2562, 2004.

[42] Fielicke, A., von Helden, G., Meijer, G., Simard, B., and Rayner, D. M. Direct observation of size dependent activation of NO on gold clusters. *Physical Chemistry Chemical Physics*, 7:3906-3909, 2005.

[43] Ma, J., Cao, X., Chen, M., Yin, B., Xing, X., and Wang, X. Low-Temperature Disproportionation Reaction of NO on Au_6^-: A Mechanism Involving Three NO Molecules Promoted by the Negative Charge. *The Journal of Physical Chemistry A*, 120:9131-9137, 2016.

[44] Ma, J., Wang, T., Yang, J., Hu, J., and Xing, X. Adsorption and reactions of NO molecules on anionic gold clusters in the size range below 1 nm: effects of clusters' global electronic properties. *Physical Chemistry Chemical Physics*, 22:25227-25235, 2020.

[45] Xu, J., White, T., Li, P., He, C., Yu, J., Yuan, W., and Han, Y. F. Biphasic Pd− Au alloy catalyst for low-temperature CO oxidation. *Journal of the American Chemical Society*, 132:10398-10406, 2010.

[46] Gao, F., Wang, Y., and Goodman, D. W. CO oxidation over AuPd (100) from ultrahigh vacuum to near-atmospheric pressures: the critical role of contiguous Pd atoms. *Journal of the American Chemical Society*, 131:5734-5735, 2009.

[47] Edwards, J. K., Ntainjua N, E., Carley, A. F., Herzing, A. A., Kiely, C. J., and Hutchings, G. J. Direct synthesis of H_2O_2 from H_2 and O_2 over gold, palladium, and gold–palladium catalysts supported on acid-pretreated TiO_2. *Angewandte chemie international edition*, 48:8512-8515, 2009.

[48] Edwards, J. K., Solsona, B. E., Landon, P., Carley, A. F., Herzing, A., Kiely, C. J., and Hutchings, G. J. Direct synthesis of hydrogen peroxide from H_2 and O_2 using TiO_2-supported Au–Pd catalysts. *Journal of Catalysis*, 236:69-79, 2005.

[49] Pawelec, B., Venezia, A. M., La Parola, V., Cano-Serrano, E., Campos-Martin, J. M., and Fierro, J. L. G. AuPd alloy formation in Au-Pd/Al_2O_3 catalysts and its

role on aromatics hydrogenation. *Applied surface science*, 242:380-391, 2005.

[50] Peng, S. L., Gan, L. Y., Tian, R. Y., and Zhao, Y. J. Theoretical study of CO adsorption and oxidation on the gold–palladium bimetal clusters. *Computational and Theoretical Chemistry*, 977:62-68, 2011.

[51] Zhang, J., Jin, H., Sullivan, M. B., Lim, F. C. H., and Wu, P. Study of Pd–Au bimetallic catalysts for CO oxidation reaction by DFT calculations. *Physical Chemistry Chemical Physics*, 11:1441-1446, 2009.

[52] Begum, P. and Deka, R. C. A Comparative DFT Study on the Catalytic Oxidation of Nitric Oxide by Pd_2 and PdM (M= Cu, Rh, Ag, Au, Pt). *Catalysis Letters*, 147:581-591, 2017.

[53] Biswakarma, N., Sarma, P. J., Baruah, S. D., Gour, N. K., and Deka, R.C. Catalytic oxidation of NO on $[Au–M]^-$(M= Pd and Pt) bimetallic dimers: an insight from density functional theory approach. *The Journal of Physical Chemistry C*, 124:3059-3068, 2020.

[54] Frisch, M. J., Trucks, G. W., Schlegel, H. B., Scuseria, G. E., Robb, M. A., Cheeseman, J. R., Scalmani, G., Barone, V., Mennucci, B., Petersson, G. A., Nakatsuji, H., Li, X., Caricato, M., Marenich, A. V., Bloino, J., Janesko, B. G., Gomperts, R., Mennucci, B., Hratchian, H. P., Ortiz, J. V., Izmaylov, A. F., Sonnenberg, J. L., Williams-Young, D., Ding, F., Lipparini, F., Egidi, F., Goings, J., Peng, B., Petrone, A., Henderson, T., Ranasinghe, D., Zakrzewski, V. G., Gao, J., Rega, N., Zheng, G., Liang, W., Hada, M., Ehara, M., Toyota, K., Fukuda, R., Hasegawa, J., Ishida, M., Nakajima, T., Honda, Y., Kitao, O., Nakai, H., Vreven, T., Throssell, K., Montgomery, J. A. Jr., Peralta, J. E., Ogliaro, F., Bearpark, M. J., Heyd, J. J., Brothers, E. N., Kudin, K. N., Staroverov, V. N., Keith, T. A., Kobayashi, R., Normand, J., Raghavachari, K., Rendell, A. P., Burant, J. C., Iyengar, S. S., Tomasi, J., Cossi, M., Millam, J. M., Klene, M., Adamo, C., Cammi, R., Ochterski, J. W., Martin, R. L., Morokuma, K., Farkas, O., Foresman, J. B., Fox, D. J. Gaussian 09, Revision D. 01, Gaussian, Inc., Wallingford CT, 2009.

[55] Weigend, F. and Ahlrichs, R. Balanced basis sets of split valence, triple zeta valence and quadruple zeta valence quality for H to Rn: Design and assessment of accuracy. *Physical Chemistry Chemical Physics*, 7:3297-3305, 2005.

[56] Weigend, F. Accurate Coulomb-fitting basis sets for H to Rn. *Physical chemistry chemical physics*, 8:1057-1065, 2006.

[57] Zhao, Y. and Truhlar, D. G. A new local density functional for main-group thermochemistry, transition metal bonding, thermochemical kinetics, and noncovalent interactions. *The Journal of chemical physics*, 125:194101, 2006.

[58] Ferrighi, L., Hammer, B., and Madsen, G. K. 2D− 3D transition for cationic and anionic gold clusters: a kinetic energy density functional study. *Journal of the American Chemical Society*, 131:10605-10609, 2009.

[59] Vilhelmsen, L. B. and Hammer, B. Systematic Study of Au_6 to Au_{12} Gold Clusters on MgO (100) F Centers Using Density-Functional Theory. *Physical review letters*, 108:126101, 2012.

[60] Maitarad, P., Namuangruk, S., Zhang, D., Shi, L., Li, H., Huang, L., Boekfa, B., and Ehara, M. Metal–porphyrin: a potential catalyst for direct decomposition of N_2O by theoretical reaction mechanism investigation. *Environmental science & technology*, 48:7101-7110, 2014.

[61] Peng, C. and Bernhard Schlegel, H. Combining synchronous transit and quasi-newton methods to find transition states. *Israel Journal of Chemistry*, 33:449-454, 1993.

[62] Schlegel, H. B. Optimization of equilibrium geometries and transition structures. *Journal of computational chemistry*, 3:214-218, 1982.

[63] Gonzalez, C. and Schlegel, H. B. Improved algorithms for reaction path following: higher-order implicit algorithms. *The Journal of chemical physics*, 95:5853-5860, 1991.

[64] Foster, J. P. and Weinhold, F. Natural hybrid orbitals. *Journal of the American Chemical Society*, 102:7211-7218, 1980.

[65] Lu, T. and Chen, F. Multiwfn: A multifunctional wavefunction analyzer. *Journal of computational chemistry*, 33:580-592, 2012.

[66] Kozuch, S. A refinement of everyday thinking: the energetic span model for kinetic assessment of catalytic cycles. *Wiley Interdisciplinary Reviews: Computational Molecular Science*, 2:795-815, 2012.

[67] Kozuch, S. and Martin, J. M. What makes for a bad catalytic cycle? A theoretical study on the Suzuki− Miyaura reaction within the energetic span model. *ACS Catalysis*, 1:246-253, 2011.

[68] Kozuch, S. and Shaik, S. How to conceptualize catalytic cycles? The energetic span model. *Accounts of chemical research*, 44:101-110, 2011.

[69] Yoon, B., Häkkinen, H., and Landman, U. Interaction of O_2 with gold clusters: Molecular and dissociative adsorption. *The Journal of Physical Chemistry A*, 107:4066-4071, 2003.

[70] Liao, M. S., Watts, J. D., and Huang, M. J. Theoretical comparative study of oxygen adsorption on neutral and anionic Ag_n and Au_n clusters (n= 2–25). *The Journal of Physical Chemistry C*, 118:21911-21927, 2014.

[71] Ai-Jie, M., Xiao-Yu, K., Gang, C., Ya-Ru, Z., Yan-Fang, L., Peng, L., and Chi, Z. Ab initio calculation of the geometric, electronic and magnetic properties of neutral and anionic Au_nPd (n= 1–9) clusters. *Molecular Physics*, 109:1485-1494, 2011.

[72] Kalita, B. and Deka, R. C. Stability of small Pd_n (n= 1–7) clusters on the basis of structural and electronic properties: A density functional approach. *The Journal of chemical physics*, 127:244306, 2007.

[73] Xing, X., Hermann, A., Kuang, X., Ju, M., Lu, C., Jin, Y., Xia, X., and Maroulis, G. Insights into the geometries, electronic and magnetic properties of neutral and charged palladium clusters. *Scientific reports*, 6:19656, 2016.

[74] Lide D. R. *CRC handbook of chemistry and physics*, CRC Press, New York, 89th edition, 2009.

[75] Wiberg, K. B. Application of the pople-santry-segal CNDO method to the cyclopropylcarbinyl and cyclobutyl cation and to bicyclobutane. *Tetrahedron*, 24:1083–1096, 1968.

[76] Yang, W., Gao, Z., Liu, X., Li, X., Ding, X., and Yan, W. Single-atom iron catalyst with single-vacancy graphene-based substrate as a novel catalyst for NO oxidation: a theoretical study. *Catalysis Science & Technology*, 8:4159-4168, 2018.

[77] Gao, Z., Li, A., Liu, X., Ma, C., Li, X., Yang, W., and Ding, X. Density functional study of the adsorption of NO on Ni_n (n= 1, 2, 3 and 4) clusters doped functionalized graphene support. *Applied surface science*, 481:940-950, 2019.

[78] Liu, X., Gao, Z., Huang, H., Yan, G., Huang, T., Chen, C., Yang, W., and Ding, X. L. Simultaneous catalytic oxidation of nitric oxide and elemental mercury by

single-atom Pd/g-C_3N_4 catalyst: A DFT study. *Molecular Catalysis*, 488:110901, 2020.

[79] Biswakarma, N., Dowerah, D., Baruah, S. D., Sarma, P. J., Gour, N. K., and Deka, R. C. Catalytic oxidation of NO to NO_2 on pure and doped Au_nPt_{3-n} (n= 0–3) clusters: A DFT perspective. *Molecular Catalysis*, 515:111910, 2021.

[80] Olsson, L., Persson, H., Fridell, E., Skoglundh, M., and Andersson, B. A kinetic study of NO oxidation and NO_x storage on Pt/Al_2O_3 and Pt/BaO/Al_2O_3. *The Journal of Physical Chemistry B*, 105:6895-6906, 2001.

[81] Torres, D., González, S., Neyman, K. M., and Illas, F. Adsorption and oxidation of NO on Au (1 1 1) surface: Density functional studies. *Chemical physics letters*, 422:412-416, 2006.

[82] Narula, C. K., Allard, L. F., Stocks, G. M., and Moses-DeBusk, M. Remarkable NO oxidation on single supported platinum atoms. *Scientific reports*, 4:7238, 2014.

[83] Smeltz, A. D., Getman, R. B., Schneider, W. F., and Ribeiro, F. H. Coupled theoretical and experimental analysis of surface coverage effects in Pt-catalyzed NO and O_2 reaction to NO_2 on Pt (1 1 1). *Catalysis Today*, 136:84-92, 2008.

[84] Mulla, S. S., Chen, N., Cumaranatunge, L., Blau, G. E., Zemlyanov, D. Y., Delgass, W. N., Epling, W. S., and Ribeiro, F. H. Reaction of NO and O_2 to NO_2 on Pt: Kinetics and catalyst deactivation. *Journal of Catalysis*, 241:389-399, 2006.

[85] Wang, H. F., Guo, Y. L., Lu, G., and Hu, P. NO oxidation on platinum group metals oxides: first principles calculations combined with microkinetic analysis. *The Journal of Physical Chemistry C*, 113:18746-18752, 2009.